Fluid Dynamics &
Materials Processing

Tech Science Press

http://doi.org/10.32604/fdmp.2026.080326

REVIEW

A Systematic Review of Multiphase Flow and Phase Change in Cryogenic CH_4-CO_2 Pipeline Systems

Ting He*, Dong Chen, Liqiong Chen, Kun Huang and Haoyu Jia

Petroleum Engineering School, Southwest Petroleum University, Chengdu, China
*Corresponding Author: Ting He. Email: heting199503@163.com

Received: 06 February 2026; Accepted: 14 April 2026; Published: 27 May 2026

ABSTRACT: The global transition toward sustainable energy systems underscores the strategic importance of methane (CH_4)–carbon dioxide (CO_2) mixtures in cryogenic applications. In Liquefied Natural Gas (LNG) processing and Carbon Capture, Utilization, and Storage (CCUS) networks, such mixtures are routinely exposed to low-temperature environments where phase stability becomes critical. Under these conditions, the unintended formation of solid CO_2 (dry ice) within pipelines poses significant engineering challenges, including flow blockage and potential equipment damage. Ensuring flow assurance therefore demands a rigorous understanding of the coupling between thermodynamic phase transitions and complex hydrodynamic behavior. This paper presents a comprehensive review of recent advances in gas–liquid–solid multiphase flow and phase change mechanisms in CH_4-CO_2 systems. It analyzes the thermophysical properties governing CO_2 de-sublimation and hydrate crystallization, with particular emphasis on non-equilibrium kinetics and delayed nucleation phenomena. In addition, the study assesses the capabilities of advanced modeling approaches, including Computational Fluid Dynamics (CFD), Molecular Dynamics (MD), and Machine Learning (ML) techniques, in predicting flow regime transitions and slurry transport behavior.

KEYWORDS: Cryogenic multiphase flow; CH_4-CO_2 binary system; solid formation kinetics thermodynamic non-equilibrium

1 Introduction

Climate change has emerged as a global crisis posing an existential threat to human survival and development. To limit the global average temperature rise to 1.5°C, the International Energy Agency (IEA) has articulated the ambitious vision of "Net Zero by 2050," a mandate that necessitates a profound structural transformation of the global energy system [1]. The transition towards a carbon-neutral energy landscape relies heavily on the dual pillars of cleaner fossil fuel utilization—specifically Liquefied Natural Gas (LNG)—and the rapid deployment of Carbon Capture, Utilization, and Storage (CCUS) [2]. To limit global temperature rise, the International Energy Agency (IEA) projects a synchronized expansion of LNG trade to secure transitional energy supply and CCUS infrastructure to decarbonize industrial emissions [3]. These strategic mandates necessitate a profound transformation in global energy infrastructure, placing unprecedented demands on the safety and efficiency of fluid transport systems.

A fundamental intersection of these sectors lies in the handling of methane-carbon dioxide (CH_4-CO_2) mixtures within pipeline networks. This binary system is ubiquitous in a wide array of critical engineering scenarios where fluids operate near the thermodynamic boundaries of solid CO_2 formation:

Natural Gas Liquefaction (LNG) [4]: Raw natural gas extracted from reservoirs typically contains significant CO_2 fractions. During the liquefaction process (Fig. 1), which typically operates under high pressures (4–7 MPa) and cools the gas to deep cryogenic temperatures (111 K), even trace amounts of CO_2 can crystallize well before methane liquefies. This poses severe blockage risks in the Main Cryogenic Heat Exchanger (MCHE) and downstream rundown lines, necessitating strict CO_2 removal to <50 ppm.

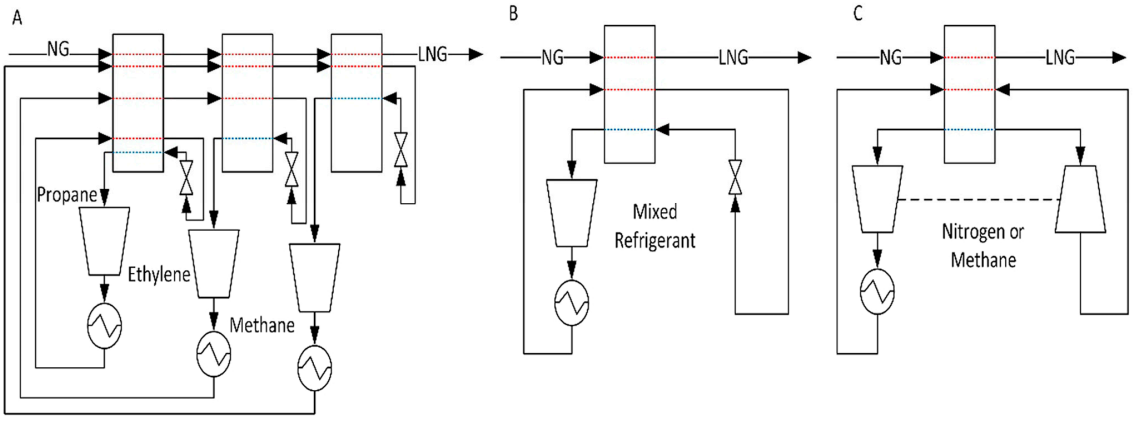

Figure 1: Schematic diagrams of the three main groups of the LNG processes. (**A**) Cascade liquefaction process, (**B**) Expansion-based processes, and (**C**) Mixed refrigerant processes.

CO_2 Transport in CCUS [5]: Captured CO_2 streams, particularly those separated during natural gas decarbonization processes, are typically transported in dense or supercritical phases to maximize efficiency. While operating under typical high-pressure (8 to 15 MPa) and near-ambient temperature (288 K to 313 K) conditions, these streams face severe phase change risks during transient operations. Rapid Joule-Thomson cooling can drastically drive the fluid temperature below the CO_2 triple point, triggering instantaneous condensation and subsequent dry ice formation. Fig. 2 illustrates the relevant CCUS process.

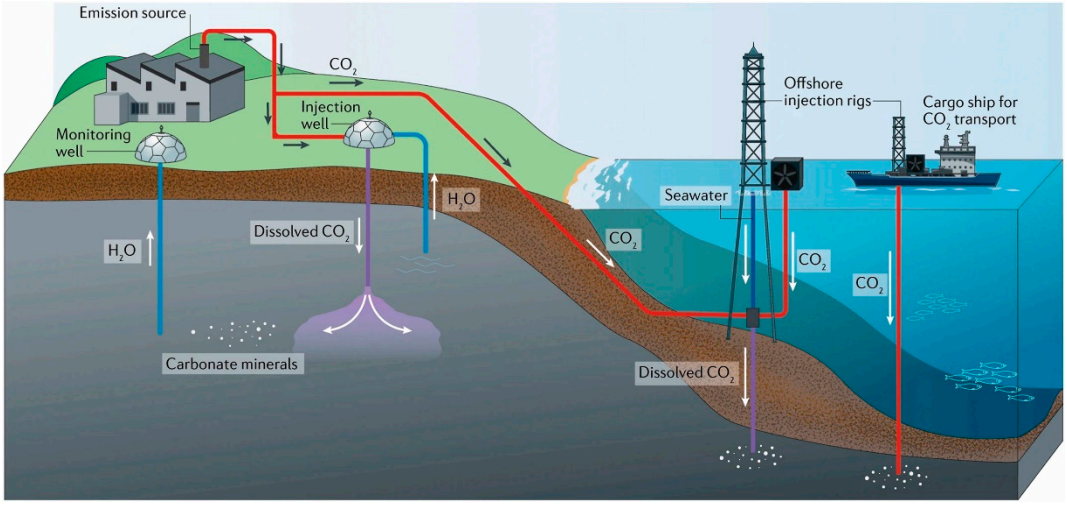

Figure 2: Schematic diagram of terrestrial and maritime CCUS integrated process. Reprinted from Ref. [6].

Cryogenic Biogas Upgrading [7]: Emerging technologies for upgrading biogas utilize cryogenic distillation to separate CO_2 from biomethane. Fig. 3 shows main cryogenic pathways for high-purity

biomethane. Unlike traditional absorption methods, this process intentionally operates at elevated pressures (1.5 to 4.0 MPa) and deep cooling temperatures (183 K to 223 K), purposefully approaching the freezing point of CO_2. The formation of solid CO_2, if not precisely controlled under these extreme conditions, can lead to severe fouling of distillation columns and piping blockages.

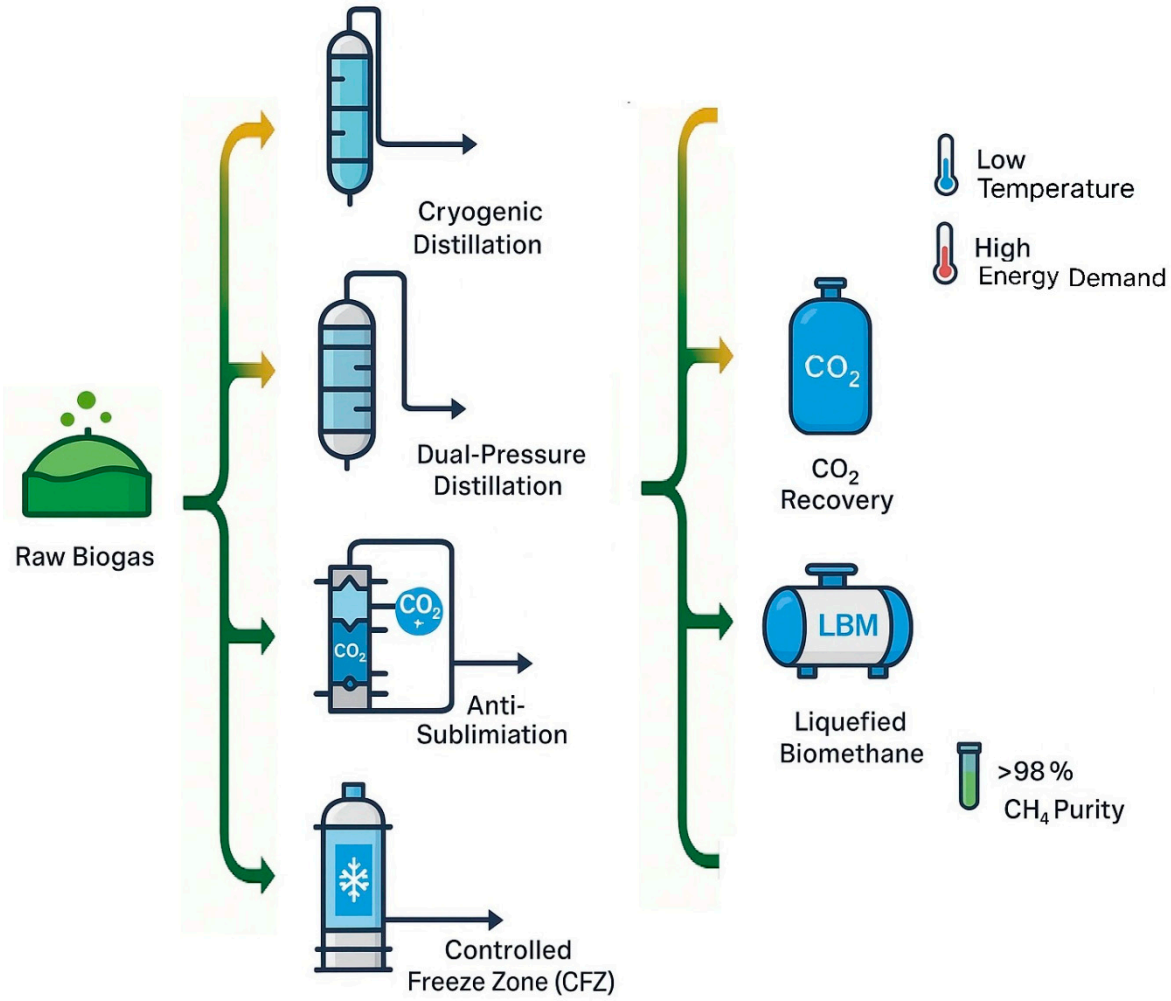

Figure 3: Main cryogenic pathways for high-purity biomethane. Reprinted from Ref. [8].

Cryogenic Carbon Capture (CCC) [9]: This technology intentionally de-sublimates CO_2 from natural gas streams to form solid CO_2 particles (Fig. 4). The initial de-sublimation typically operates at moderate pressures (0.1 to 1.0 MPa) and deep cryogenic temperatures (138 K to 173 K). These solids are subsequently melted and highly pressurized (10 to 15 MPa) for efficient delivery. The intervening transport of solid CO_2 slurries within the process piping represents a deliberate application of gas-liquid-solid flow, where flow assurance is paramount.

CO_2-Rich Associated Gas Reinjection [10]: In offshore oil fields, associated gas with high CO_2 content is often reinjected into reservoirs to avoid flaring. Operating at exceptionally high pressures (20 to 40 MPa) and moderate surface temperatures (293 K to 333 K), the injection lines experience extreme cooling effects when subjected to substantial pressure drops across choke valves. This rapid Joule-Thomson expansion can cause local temperatures to plummet below the CO_2 triple point (216.5 K). Without adequate heating, dry ice can precipitate within the injection manifolds, compromising well injectivity. In all these contexts, the

pipeline systems must operate under stringent cryogenic or high-pressure conditions. Accurate prediction of the phase behavior and flow dynamics of the CH_4-CO_2 system is therefore the cornerstone of maintaining mechanical integrity and ensuring continuous operation.

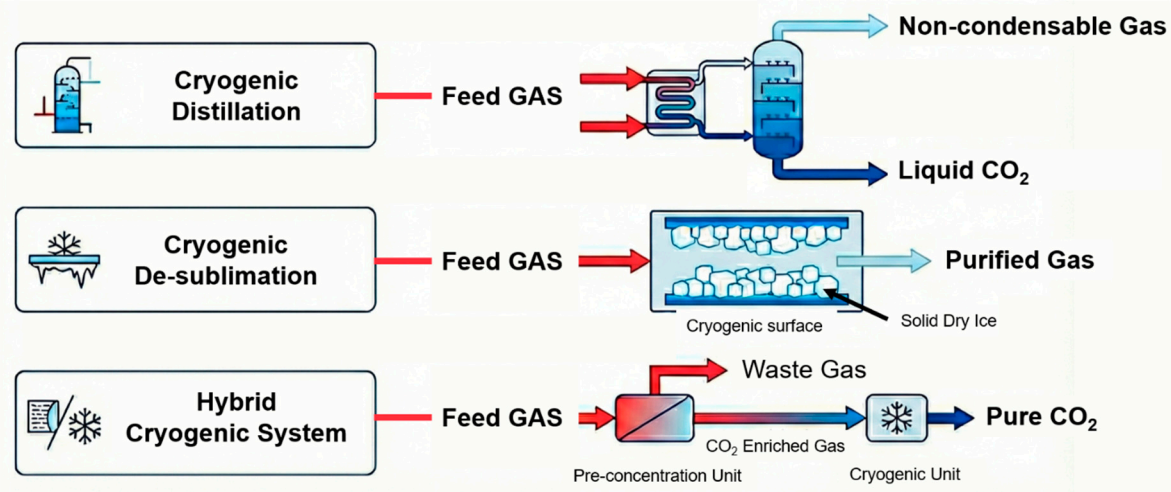

Figure 4: Cryogenic Carbon Capture technology.

However, the transition to accurate predictive capability reveals a significant uncertainty regarding the dynamic evolution of gas-liquid-solid flows. While the thermodynamic boundaries of solid formation (dry ice) are relatively well-mapped, a critical knowledge gap exists concerning the hydrodynamic behavior of the resulting multiphase flow. Once solid particles emerge within the pipeline—triggered by operational temperature drops or accidental rapid depressurization—the system transitions from a conventional two-phase flow to a complex particulate suspension. The presence of the solid phase fundamentally disrupts established flow regimes and transport laws. Existing mechanistic models, originally developed for gas-liquid flows, often fail to predict critical parameters in this three-phase environment, such as: Pressure drop anomalies caused by slurry viscosity changes. Particle agglomeration kinetics that lead to sudden plug formation. Threshold velocities required to prevent bed deposition. The lack of a unified understanding of how phase change kinetics couple with flow hydrodynamics remains the primary barrier to preventing catastrophic blockages in these critical infrastructures.

Despite the critical importance of this domain, existing literature remains fragmented. Previous reviews have predominantly focused on either the phase equilibrium thermodynamics of CH_4-CO_2 mixtures or the general multiphase flow characteristics in conventional oil and gas pipelines at ambient temperatures. Comprehensive surveys that bridge the gap between cryogenic phase change mechanisms and the resulting gas-liquid-solid flow dynamics are notably scarce. Specifically, a systematic synthesis connecting microscopic interactions (e.g., heat and mass transfer during solidification) to macroscopic flow behaviors in the specific context of cryogenic temperatures is currently lacking.

To bridge this gap, this review aims to systematically comprehensively survey the gas-liquid-solid flow behaviors and phase change mechanisms of the CH_4-CO_2 system in pipelines. To ensure research precision, this review assumes sufficient dehydration has occurred to exclude hydrate formation, thereby focusing exclusively on the crystallization and transport of solid CO_2 (dry ice). The scope encompasses the cryogenic temperature range, focusing on the interplay between flow dynamics, thermodynamics, and solid transport.

Section 2 establishes the thermodynamic foundation. It reviews thermophysical properties, phase equilibria, and the critical conditions for solid CO_2 formation.

Section 3 examines macroscopic flow behavior. It summarizes experimental findings on flow regimes, transition mechanisms, and the physics of solid particle transport and deposition.

Section 4 investigates coupled mechanisms. It analyzes heat and mass transfer during phase changes, interactions between solid-liquid-gas phases.

Section 5 evaluates modeling approaches. It covers methods ranging from thermodynamic Equations of State (EOS) to Computational Fluid Dynamics (CFD), highlighting current limitations in predicting solid formation.

Finally, the paper summarizes current challenges and proposes future research directions to enhance the safety and efficiency of cryogenic pipeline networks.

2 Study Selection and Research Landscape

The study selection process followed PRISMA guidelines to ensure transparency and reproducibility. A total of 327 records were identified through database searches (Web of Science, ScienceDirect, Scopus, Engineering Village) and manual screening. After removal of 91 duplicates and the application of predefined inclusion and exclusion criteria, 116 studies were retained for final synthesis (Fig. 5). To systematically evaluate the current research landscape, the included literature was broadly categorized by methodology: 58 articles primarily utilized numerical and theoretical modeling, whereas 45 papers were driven by experimental measurements, providing a comprehensive basis for comparing simulated predictions with empirical data.

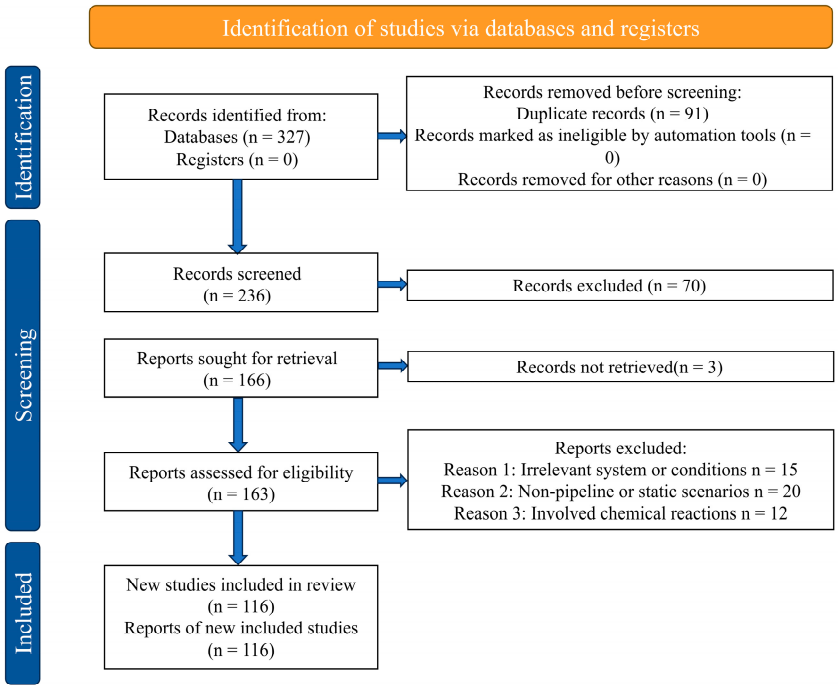

Figure 5: PRISMA 2020 flow diagram detailing the systematic identification, screening, eligibility assessment, and inclusion of studies in the review of multiphase flow and phase change in cryogenic CH_4-CO_2 pipeline systems. Numbers reflect the sequential filtering from initial records identified (n = 327) through duplicate removal, title/abstract screening, full-text review, and final inclusion (n = 116 studies).

3 Fundamentals of CH_4-CO_2 Systems at Low Temperatures

Accurate thermodynamic prediction underpins all analyses of cryogenic in-pipe multiphase flows. Unlike ambient flows, the cryogenic CH_4-CO_2 system exhibits complex phase behaviors, encompassing vapor-liquid equilibrium (VLE), solid-vapor equilibrium (SVE), and solid-liquid-vapor equilibrium (SLVE) equilibria. The formation boundary of solid CO_2 is defined not by a fixed temperature point, but by a dynamic envelope varying with pressure and composition. Unlike conventional oil-water flows, this system is governed by extreme temperature gradients and its proximity to the CO_2 triple point. In this region, even slight thermodynamic fluctuations can trigger abrupt phase transitions. The phase transition characteristics of the cryogenic CH_4-CO_2 system have been the subject of extensive experimental and theoretical investigation. Yet, parallel to the advancement of CCUS and cryogenic industries, the scientific focus has progressively shifted towards high-CO_2-content mixtures and deep cryogenic environments. In light of this evolution, this section provides a systematic summary of the phase behavior and highlights the emerging developmental trends of the CH_4-CO_2 binary system under low-temperature conditions.

3.1 Thermophysical Properties and Non-Equilibrium Phase Behavior

The accurate prediction of flow regimes and pressure drops relies fundamentally on the thermodynamic state properties of the fluid mixture. The CH_4-CO_2 system exhibits complex phase behavior characterized by a wide distillation gap between triple point discrepancy. Extensive experimental and theoretical research has been conducted to map the phase boundaries of this binary system. The triple point of pure CO_2 is located at T_t = 216.58 K and P_t = 0.518 MPa. However, in CH_4-rich mixtures, intermolecular interactions induce significant shifts in phase boundaries [11]. The CO_2-CH_4 binary system is categorized as a Type I system under cryogenic conditions [12], characterized by a continuous gas-liquid critical line connecting the critical points of pure CH_4 and CO_2. The solid-vapor-liquid equilibrium (SVLE) connects the triple points of the two pure components, exhibiting a distinct pressure maximum near the CO_2 triple point. The domain bounded by the critical line and the SVLE curve defines the region of vapor-liquid equilibrium (VLE), as shown in Fig. 6:

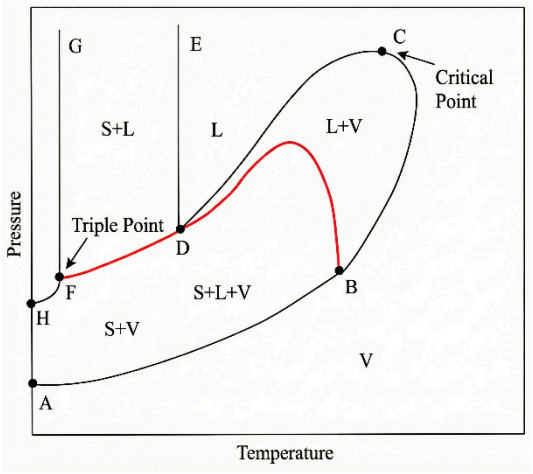

Figure 6: Phase Diagram of the CO_2-CH_4 System.

Ref. [13] summarized the qualitative P-T phase diagram, where phase boundaries are defined by the triple-point locus and the freeze-out region. Extensive theoretical and experimental investigations have been

conducted to characterize the thermodynamic properties of the CH_4-CO_2 binary mixture under cryogenic conditions. The key phase transition parameters reported in the literature are summarized in Table 1.

Table 1: Experiment on the thermodynamic properties of the CH_4-CO_2 binary system.

Ref.	T/K	P/MPa	CO_2 Comp.	Phase Equil. Type	Exp. Method	Key Remarks
[14]	195–289	0.9–8.6	0.18–0.88	VLE, SVE, SLVE	Visual cell; Vapor circulation	Mapped the SLVE locus; Identified solid CO_2 intrusion into VLE region.
[15]	133–210	0.16–4.8	0.01–0.2	SVE, SLVE, VLE	Static-synthetic; Static-analytic	Major SVE data source for GPSA Data Book; Resolved low-temp discrepancies of D&K.
[11]	98–216.6	0.03–4.9	0.001–0.2	SLVE, SLE, SVE	Vapor recirculation; Visual crystal-point	Extends SLVE locus to 98 K; Reported impurity N_2 effects.
[16]	144–216	0.5–5.5	0.02–0.9	SLVE, SVE, SLE	Static-analytic	multicomponent data (C_1–C_3).
[17]	196–210	0.29–4.45	0.108–0.542	SVE	Isochoric method	Fills the gap for medium-to-high CO_2 content.
[18]	83–123	Atm.	2–500 ppm	SLE	Static-analytic	Key solubility data for LNG temperatures.
[19]	204–303	up to 9	0.02–0.95	VLE, SLVE	Static-analytic	Sour gas focus.

Note: VLE: vapor-liquid equilibrium; SVE: solid-vapor equilibrium; SLVE: solid-liquid-vapor equilibrium; SLE: Solid-Liquid Equilibrium.

Early experimental studies established the fundamental phase diagram of the CH_4-CO_2 system. Donnelly and Katz [14] pioneered measurements of the critical and triple-point loci across 195–289 K and 0.9–8.6 MPa, revealing for the first time the pressure maximum of the three-phase curve within the vapor-liquid equilibrium region. Pikaar and James [15] subsequently expanded the experimental envelope to 113.15 K and 10.13 MPa, employing a combination of sampling and non-sampling techniques to determine vapor-liquid, solid-vapor, and solid-liquid equilibria for mixtures containing 1–20% CO_2. Davis, Rodewald [11] extended measurements of the solid-liquid-vapor equilibrium (SLVE) locus down to 97.54 K, detailing vapor-liquid compositions for low-CO_2 mixtures. Kurata and Im (16) utilized sampling techniques to supplement vapor-liquid equilibrium composition data in the presence of the solid phase across the 144–216 K. Wichterle and Kobayashi [20] systematically measured data for seven isotherms across the 153.15–219.26 K range. It rectified deviations in liquid-phase activity coefficient calculations, providing a critical foundation for predicting pre-freeze-out liquid compositions.

Driven by CCUS initiatives and high-acid gas field development requirements, research has expanded to encompass high CO_2 concentrations. Zhang et al. [17] measured solid-vapor equilibrium (SVE) data for mixtures with high CO_2 concentrations (10.8–54.2%) across 196.5–210.3 K, bridging data gaps in this high-concentration regime. Souza et al. [19] utilized modern analytical instrumentation to remeasure full-range VLE and SLVE data from the CO_2 triple point to the critical region, establishing the complete critical locus and identifying significant deviations in conventional models within the near-critical zone.

As cryogenic processes advance toward lower temperatures, rudimentary vapor-liquid equilibrium analyses have become insufficient, prompting a shift in modern research toward extreme operating conditions and non-isocompositional measurements to transcend early data limitations. Raposa et al. [21] introduced a non-isoplethic protocol for cryogenic binaries, this continuous-injection technique offers a promising pathway to rapidly map the deep-cryogenic region of the CH_4-CO_2 system in future. Waage,

Vlugt [22] calculated the three-phase equilibrium lines for methane and carbon dioxide hydrates across a pressure range of 50–4000 bar by utilizing molecular Monte Carlo simulations coupled with specific potential models. Aimoli et al. [23] assessed the applicability of Monte Carlo (MC) simulations versus Equations of State (EOS) for calculating phase equilibria under extreme pressures, finding that while distinct force fields and combining rules yielded equivalent, accurate results at 230 K, significant deviations emerged at 270 K. Al Ghafri et al. [24] determined vapor-liquid, vapor-liquid-liquid (VLLE), and four-phase vapor-liquid-liquid-hydrate equilibrium data for the ternary methane-carbon dioxide-water system using a high-pressure quasi-static apparatus; their analysis revealed that CO_2 significantly enhances n-alkane solubility in the aqueous phase compared to binary systems. Eniolorunda et al. [25] investigated the impact of CO_2 composition variations (30–73 mol%, up to 24 MPa) on global solid-fluid phase transitions, acquiring equilibrium data under both saturated and undersaturated conditions. Ahmed [26] developed a Response Surface Methodology (RSM) model to predict binary phase behavior; results indicate that under low-temperature, high-pressure conditions, methane predominates in the gas phase while CO_2 concentrates in the liquid, with the reverse distribution observed at high temperatures and low pressures. Employing High-Pressure Micro-Differential Scanning Calorimetry (HP-μDSC), Robustillo et al. [27] characterized CH_4-CO_2 hydrate phase transition temperatures across varying compositions up to 100 MPa, finding these transition characteristics largely insensitive to water content or thermal scanning rates.

Current research predominantly focuses on the fundamental CH_4-CO_2 binary system (as summarized in Table 1). However, it is worth noting that trace heavy hydrocarbons, as investigated by Simoncelli et al. [28], can induce complex liquid-liquid immiscibility. While beyond the scope of this review, future work should address how these multicomponent interactions impact the baseline binary phase envelope established here.

3.2 Phase Change Phenomena: Crystallization and De-Sublimation

Solid precipitation in the cryogenic CH_4-CO_2 system constitutes a complex process involving multiscale physical mechanisms [29]. The fundamental driving force for phase transitions stems from the Gibbs free energy differential between the parent and nascent phases. In engineering contexts, this potential is typically quantified via the supersaturation ratio (S) [30,31]. Understanding how solids form is as important as knowing when they form. While temperature, pressure, and surface characteristics each exert distinct mechanistic influences on the initial condensation process, the subsequent formation of solid CO_2 in pipelines is not a singular phenomenon [32]; rather, it occurs via two distinct thermodynamic pathways determined by the local pressure relative to the CO_2 triple point. Understanding the difference (Table 2) between crystallization and de-sublimation is crucial for elucidating the underlying flow mechanisms.

Table 2: Differences between crystallization and de-sublimation.

Feature	Crystallization	De-Sublimation
Primary Medium	Liquid CH_4 dominant (LNG)	Gaseous/Supercritical streams (CCUS)
Formation Site	Bulk fluid volume	Pipe walls or Expansion cores
Resulting Solid	Discrete particles/Agglomerates	Fixed layers/Snow-like flakes
Flow Risk	Sedimentation & Viscosity rise	Diameter restriction & Layer detachment

3.2.1 Crystallization

This phenomenon occurs when a liquid mixture is cooled below its Solid-Liquid Equilibrium (SLE) boundary while maintaining a pressure above the triple point pressure. As temperature drops, the solubility

of CO_2 in the liquid solvent decreases. When the concentration of CO_2 exceeds this solubility limit, the solution becomes supersaturated. The driving force for nucleation is the degree of subcooling. Once the metastability limit is breached, CO_2 molecules segregate from the liquid phase to form solid crystals. This mechanism is predominant in LNG production lines and sub-cooled liquid transport where the fluid is continuous liquid.

Fig. 7 presents the solubility curve of solid CO_2 in saturated liquid methane [33]. Rather than a simple linear decline, the data reveals a severe exponential reduction in CO_2 solubility as the system approaches deep-cooling temperatures. From an engineering perspective, this curve strictly defines the absolute operational boundary for LNG production risk. As the fluid temperature drops below 163 K, the solubility plummets abruptly into the parts-per-million (ppm) range. This physical phenomenon dictates that even microscopic trace amounts of CO_2—residual from upstream sweetening units—will inevitably reach supersaturation and precipitate as solid crystals. Consequently, this exponential decay offers precise thermodynamic grounds for why strict upstream pre-treatment (requiring CO_2 removal to <50 ppm) is essential to prevent MCHE blockages.

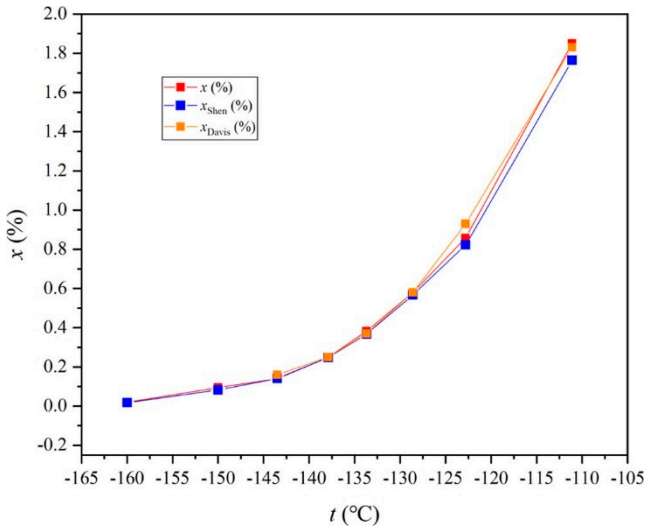

Figure 7: CO_2 Solubility in saturated liquid methane. Reprinted with permission from Reference [33]. Copyright © 2021 American Chemical Society.

Driven by the supersaturation of CO_2 in liquid methane, nucleation occurs within the bulk fluid (homogeneous nucleation) or on suspended impurities (heterogeneous nucleation). Unlike water freezing which often starts at walls, CO_2 crystallization in turbulent LNG flows tends to generate a volumetric dispersion of discrete crystals. Research indicates that CO_2 crystals formed in liquid methane typically exhibit compact, polyhedral structures. However, under high sub-cooling rates, dendritic growth may occur. Crucially for flow mechanics, these nascent crystals are often in the micrometer range but possess high surface energy, leading to rapid agglomeration into larger clusters. Since crystallization occurs throughout the fluid volume, the resulting flow regime is initially a solid-liquid suspension. The primary hydrodynamic challenges here are the modification of effective fluid viscosity and the risk of particle settling if the flow velocity drops below the critical suspension velocity.

3.2.2 De-Sublimation

De-sublimation describes the direct phase transition of CO_2 from the vapor phase to the solid state. This phenomenon is thermodynamically governed by the Solid-Vapor Equilibrium (SVE) region. In the context of cryogenic CH_4-CO_2 transport, determining the precise onset of de-sublimation is critical for defining the safe operating envelope. Fig. 8 [34] illustrates the thermodynamic boundaries of this transition through pressure-composition isotherms. The "frost point isotherms" shown in the diagram represent the solubility limit of solid CO_2 in the methane-rich vapor phase. Any thermodynamic trajectory crossing these isotherms into the two-phase region will result in the immediate precipitation of solid CO_2 crystals on pipe walls or valve surfaces.

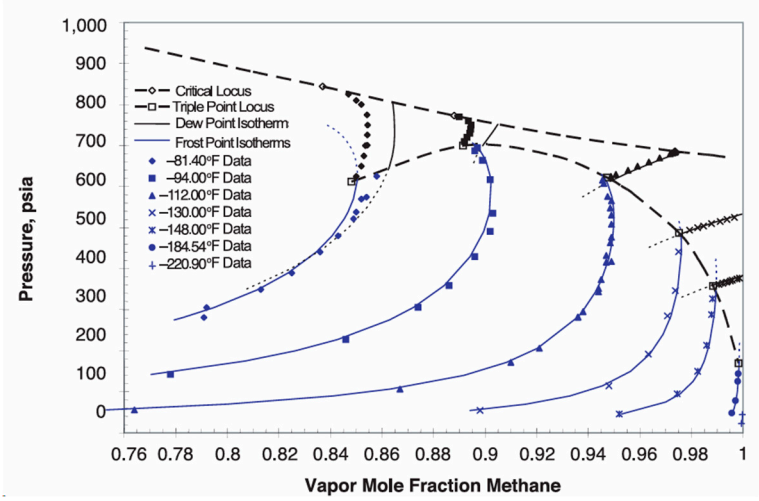

Figure 8: Frost point and dew point isotherms for the CH_4+CO_2 binary system. Reprinted from Ref. [34].

The fundamental driving force for phase transitions stems from the Gibbs free energy differential between the parent and nascent phases. In engineering contexts, this potential is typically quantified via the supersaturation ratio (S). The critical supersaturation for cryogenic CO_2 de-sublimation is influenced by temperature, gas velocity, and surface porosity. Lattice Boltzmann Method (LBM) investigations reveal that the de-sublimation regime is governed by the Péclet number (Pe) and subcooling (ΔT), which can be seen in Fig. 9; the transition from convection-limited to de-sublimation-limited states occurs at a critical Pe, significantly impacting capture rates and frost morphology [35,36]. Fig. 8. Regime map of CO_2 de-sublimation morphologies obtained from LBM simulations. The diagram identifies the critical Péclet number (Pe) and subcooling degree that mark the transition from convection-limited dendritic growth to diffusion-limited compact growth.

Wang et al. [37] uses molecular simulations illustrate the condensation and crystallization behavior of high-pressure CH_4-CO_2 binary gases on the heat exchanger surfaces. Fig. 10 illustrates how CO_2 clusters evolve during the condensation process. It shows that solid precipitation at high pressures is driven by a competition between CO_2 and CH_4 molecules. At first, CO_2 molecules gather to form clusters. However, as the temperature decreases further, the CH4 molecules start to group together rapidly, which physically breaks apart the existing CO_2 clusters and forces the CO_2 molecules to dissolve back into the gas. In engineering practice, this 'dissolution-aggregation' cycle is very important because it explains why wall-frosting in heat exchangers is sometimes delayed. Understanding this process suggests that by

carefully controlling the cooling rate, engineers might be able to extend this dissolution phase and delay the buildup of solid CO_2 on the equipment.

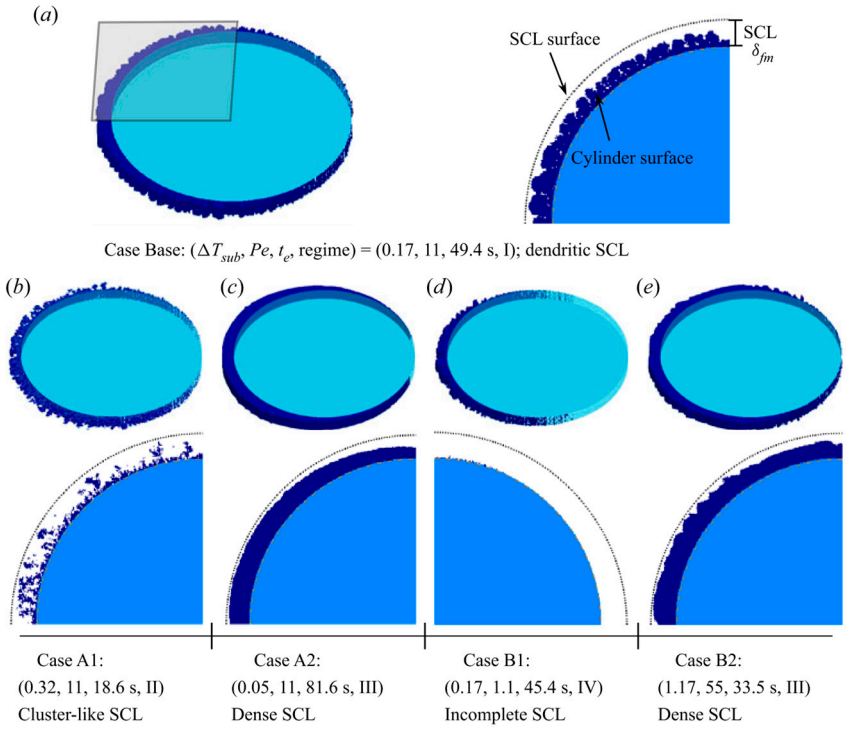

Figure 9: CO_2 de-sublimation properties in three dimensions. Contours of solid CO_2 and zoom-in views of SCL in cases. (**a**) Base, (**b**) A1, (**c**) A2, (**d**) B1 and (**e**) B2. The four de-sublimation regimes are joint-controlled (I), diffusion-controlled (II), de-sublimation-controlled (III) and convection-controlled (IV). Reprinted from Ref. [35].

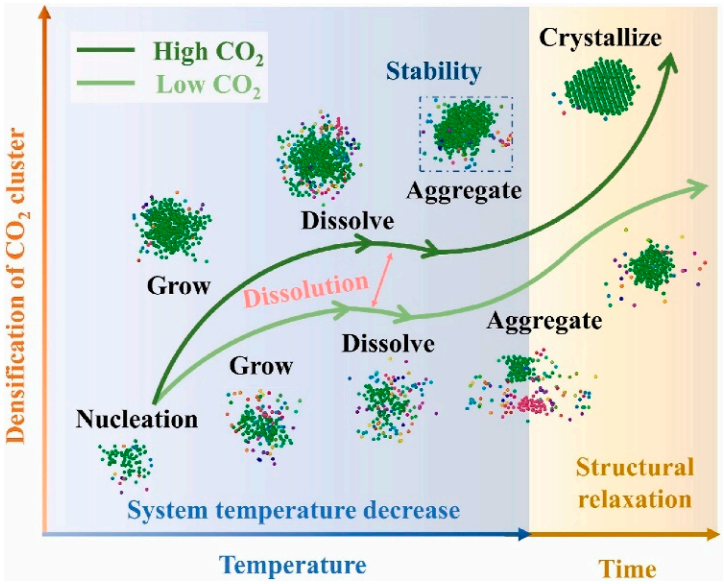

Figure 10: Dynamic pathways of CO_2 clusters evolution during CH_4-CO_2 binary gas condensation.

3.2.3 Nucleation Mechanisms: Competition between Homogeneous and Heterogeneous Nucleation

Nucleation is the process wherein a nascent phase forms critical nuclei within a metastable parent phase by surmounting the thermodynamic energy barrier. Within cryogenic natural gas pipelines, both homogeneous and heterogeneous nucleation regimes frequently coexist; however, the dominant mechanism is strictly governed by the local supersaturation field and interfacial characteristics [38].

While heterogeneous nucleation generally requires a lower activation energy due to the presence of pre-existing interfaces (such as previously condensed micro-droplets in the flow), homogeneous nucleation occurs spontaneously within the bulk fluid, isolated from boundary effects. This interstitial homogeneous nucleation becomes the primary driver of phase change under the high subcooling and rapid expansion conditions typical of supersonic separators. According to Classical Nucleation Theory (CNT) [39], the homogeneous nucleation rate $\mathcal{J}_{\text{hom}}$ exhibits a pronounced exponential sensitivity to the supersaturation ratio S, as defined in Eq. (1):

$$J_{\text{hom}} = A \cdot \exp\left(-\frac{16\pi\sigma^3 v_s^2}{3(k_B T \ln S)^2}\right) \tag{1}$$

This implies that homogeneous nucleation necessitates elevated supersaturation levels to surmount the nucleation energy barrier [40,41]. Traditional models like uncorrected CNT exhibit severe limitations in dynamic flows, underestimating nucleation rates by 3 to 4 orders of magnitude compared to molecular dynamics (MD) simulations [42]. MD reveals that during rapid expansion, CO_2 nucleation is dynamically driven by monomer collisions and Lennard-Jones energy reduction. The subsequent latent heat release creates a localized thermal non-equilibrium, leaving newly formed CO_2 clusters 10–2077 K hotter than the surrounding CH_4 and subjected to rapid condensation-evaporation cycles. This profound discrepancy highlights the necessity of coupling macro-thermodynamic variables with molecular-level kinetics to fundamentally correct classical nucleation models for CH_4-CO_2 systems.

Heterogeneous nucleation denotes the phenomenon where the nascent phase initiates on substrates such as pipeline walls or impurity particle surfaces; acting as nucleation sites, these surfaces effectively attenuate the nucleation energy barrier. Modulated by factors such as interaction strength and structural compatibility between the foreign substrate and the crystalline phase, this mechanism typically proceeds at supersaturation levels significantly lower than those required for the homogeneous pathway [43,44]. Its nucleation energy barrier ΔG^*_{het} correlates with the homogeneous counterpart through the contact angle factor $f(\theta)$, as expressed in Eq. (2):

$$\Delta G^*_{het} = \Delta G^*_{\text{hom}} \cdot f(\theta), f(\theta) = \frac{(2+\cos\theta)(1-\cos\theta)^2}{4} \tag{2}$$

where θ denotes the contact angle of the nascent phase on the substrate. For most cryogenic metallic surfaces, $\theta < 180^\circ$, resulting in a geometric factor $f(\theta)$ significantly less than 1; this diminished energy barrier, coupled with the presence of catalytic surfaces, renders heterogeneous nucleation energetically more favorable than homogeneous nucleation in cryogenic pipeline environments [38,45,46]. Recent molecular dynamics (MD) studies [47] provide a deeper microscopic perspective on this process, highlighting that this contact angle θ is fundamentally governed by interfacial wettability. The kinetic interaction energy (fluid-solid affinity) directly dictates this reduced barrier, facilitating the rapid, localized aggregation of CO_2 molecules at the interface.

4 Multiphase Flow Behavior in Low-Temperature CH_4-CO_2 Pipelines

To define the safe design boundaries of CH_4-CO_2 pipelines, it is imperative to quantify the limits of multiphase flow and solid slurry transport. While specialized facilities have provided valuable benchmarks, experimental research is currently bifurcated between microscopic and macroscopic scales. Micro-scale visualization has matured, yet macro-scale hydrodynamics are typically inferred from indirect metrics like pressure drop [48]. Direct observation of flow patterns is severely limited by cryogenic optical impediments, including window frosting and refractive index mismatches, which compromise techniques like PIV. Consequently, while wall-frosting mechanisms are relatively well-documented, the hydrodynamics of bulk slurry suspension remain unknown in current literature.

4.1 Experimental Studies

Experimental investigation remains the definitive standard for validating multiphase flow models, particularly in the complex cryogenic environment of CH_4-CO_2 systems where thermodynamic phase changes are tightly coupled with hydrodynamics. This section provides a systematic review of existing experimental campaigns, spanning from controlled laboratory-scale apparatus to industrial-relevant pilot-scale flow loops. The discussion focuses on three critical dimensions: the evolution of flow loop design and instrumentation capabilities (including PIV and high-speed imaging), the characterization of macroscopic flow regimes, and the quantitative analysis of pressure gradients and heat transfer data. By synthesizing findings across varying scales, we aim to delineate the current boundaries of empirical knowledge and highlight the consistency—or divergence—among reported results.

4.1.1 Flow Loops and Scale: From Laboratory Loops to Pilot Scale-up

Existing research has largely focused on two-phase flow and venting processes in pipelines using pure CO_2 or CO_2-rich systems. Although the working fluid composition differs from that of low-temperature CH_4-CO_2 binary systems, these studies provide important references for experimental setup design concepts and scale-up criteria.

Laboratory-scale studies typically focus on mechanism exploration and flow pattern construction. Typical devices include: IFE CO_2 flow loop (Fig. 11): This device uses a horizontal or near-horizontal pipe section with an inner diameter of 44 mm, and the test conditions cover the two-phase region. As a small-scale platform for large test lines, this loop is widely used for the refined measurement of liquid holdup, pressure drop, and flow pattern [49]. Focusing on the gravity stratification effect within horizontal pipes and eliminating interference from the vertical gravity gradient, it is suitable for studying the transition mechanism from stratified flow to slug flow.

FALCON vertical loop (Fig. 12) also uses an inner diameter of 44 mm, including a riser section of 13.7 m in height. The device carried out two-phase CO_2 upflow and downflow experiments at a pressure of 6.5 MPa, and focused on obtaining liquid holdup, pressure drop and flow pattern data in the vertical pipe section [50]. Compared to horizontal loops, FALCON fills the gap in cryogenic fluid flow in vertical pipe sections. It can directly compare the significant differences in liquid holdup and pressure drop characteristics between upflow and downflow, which is crucial for the flow assurance design of subsea pipeline riser sections.

To investigate leakage and flow control behavior in high-pressure CO_2 pipelines, several studies [51] have employed pipeline venting and pressure reduction experimental systems with inner diameters of 15–30 mm and lengths of 14–23 m, equipped with leakage nozzles of specific sizes for simulation studies. These devices are specifically designed to study the rapid temperature drop caused by the Joule-Thomson effect. Due to their small diameter and low thermal inertia, these devices can sensitively capture phase

transitions and choked flow behavior at throttling points during rapid decompression, making them an ideal platform for verifying phase transition kinetic models.

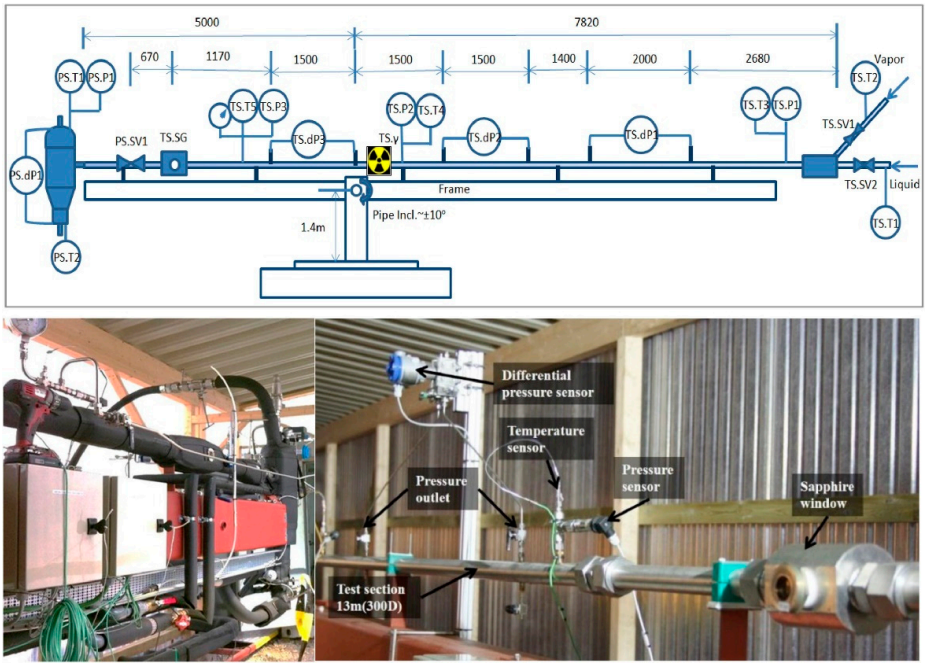

Figure 11: IFE CO_2 flow loop. Reprinted from Ref. [49].

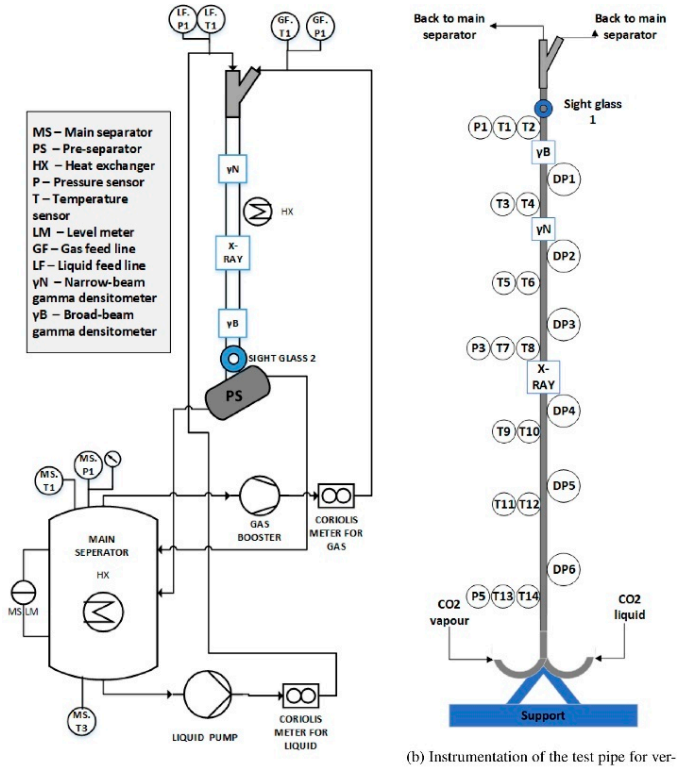

(a) Process design layout for vertical downward flow with indication of the gamma densitometers and X-ray locations,

(b) Instrumentation of the test pipe for vertical upward experiments with indication of instrument locations.

Figure 12: Schematic of the FALCON test facility (**a**,**b**). Reprinted from Ref. [50].

In order to verify the industrial applicability of laboratory data, some studies have carried out pilot-scale experiments for cross-scale comparative analysis: IFE's study compared data from a 44 mm CO_2 loop with test lines with larger diameters based on similarity criteria. The results showed that, while keeping dimensionless parameters (especially gas-liquid density ratio) consistent, liquid holdup and pressure drop exhibited good scalability [49]. On the other hand, industrial or near-industrial scale pipelines (Fig. 13) have been used for empirical studies on CO_2 release and throttling. Comparison with laboratory loops in terms of temperature extremes and phase change paths revealed that although both systems exhibit consistent overall trends in rapid decompression, drastic temperature drops, and phase evolution (two-phase or solid-phase formation), certain deviations still exist in the pressure drop waveform and minimum temperature extremes after scaling up [52,53].

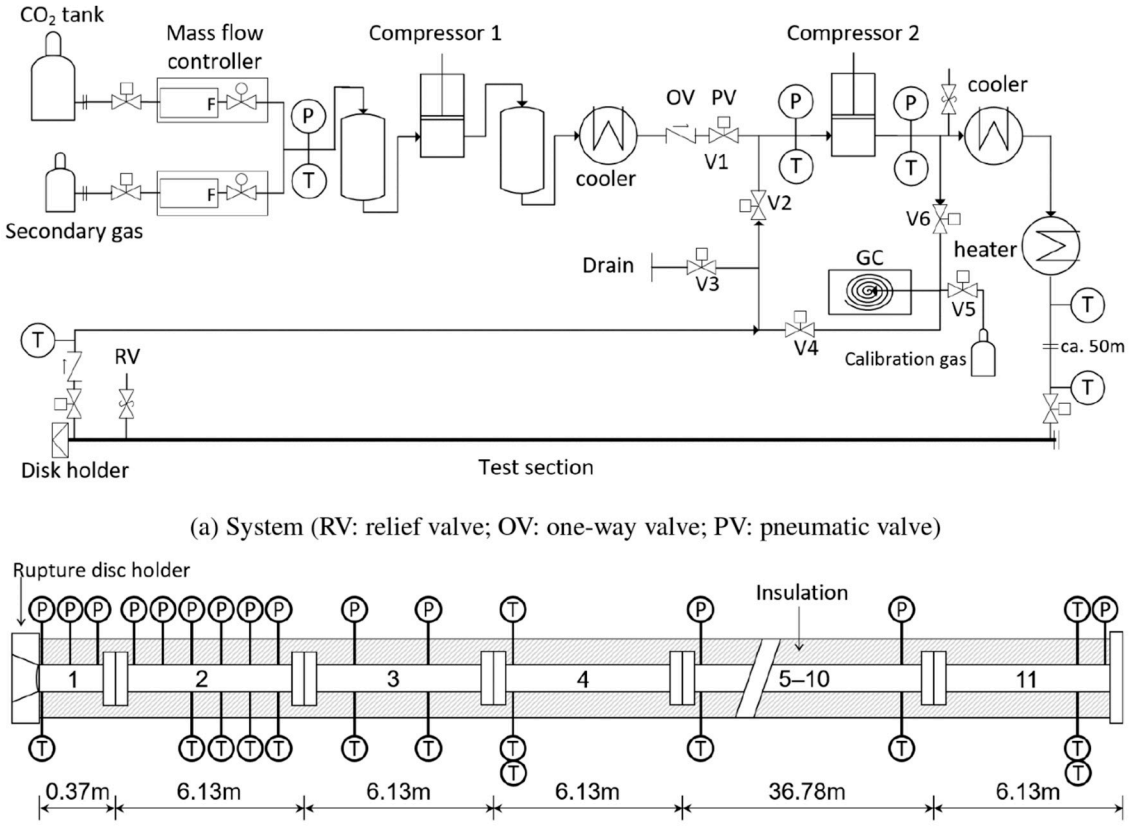

(a) System (RV: relief valve; OV: one-way valve; PV: pneumatic valve)

(b) Test section (dimensions are not to scale; pipe no. 5–10 and corresponding sensors are omitted.)

Figure 13: Schematic of the ECCSEL depressurization facility. (**a**) Schematic view of the ECCSEL depressurization facility; (**b**) Test section. Reprinted from Ref. [52].

Overall, after reasonable dimensionless analysis, the laboratory scale can represent the pilot/industrial scale well in terms of flow pattern, liquid holdup, and average pressure drop. However, for extreme phenomena such as transient decompression and local freezing, verification with pilot-scale or field data is still needed.

4.1.2 Laboratory-Scale Experiments

In current CO_2 and related cryogenic pipeline experiments, traditional optical observation is limited due to the unique characteristics of high-pressure and cryogenic conditions. Therefore, multiphase interface capture and flow field parameter measurement mainly rely on the complementary application of X-ray attenuation technology, high-frequency dynamic sensors, and microscopic visualization methods.

1. Ray attenuation method: For measuring phase distribution in opaque pipelines, X-ray or γ-ray systems are the mainstream choice. In vertical two-phase CO_2 flow, this technique is used to accurately measure axial liquid holdup distribution and determine the degree of gas-liquid slip by comparing it with the "uniform flow assumption" [50]. IFE's horizontal/near-horizontal pipeline experiments also employ X-ray technology combined with differential pressure sensors to achieve simultaneous acquisition of liquid holdup and pressure drop [49].
2. High-frequency thermal-hydraulic measurements: To capture wave propagation, throttling cooling, and phase change dynamics during transient venting, high-frequency (up to 1 kHz) pressure and temperature sensors are typically installed along the experimental pipeline. Furthermore, by measuring wall heat flux density and wall temperature, the local heat transfer coefficient and Nusselt number can be indirectly derived, enabling a quantitative characterization of the unsteady-state flow heat transfer behavior within the leak section [54].
3. Exploring the Applicability of Visualization and PIV: Existing literature reports few macroscopic PIV or visual window experiments on high-pressure, low-temperature CH_4-CO_2, mostly limited to radiographic diagnosis of opaque pipelines. However, in microscale studies (such as porous media microchannels), microscopic visualization and high-speed imaging have been successfully used to resolve fingering phenomena and residual oil distribution in the CO_2-oil-water three-phase system [55].

Current measurement technologies are well capable of meeting the requirements for obtaining macroscopic average parameters (liquid holdup, pressure drop, wall temperature). Although there are still gaps in the measurement of velocity vectors in macroscopic flow fields, the application of microscopic visualization techniques demonstrates significant feasibility and research potential for extending these techniques to the observation of CH_4-CO_2 flow patterns and the measurement of local velocity fields (PIV) in small-diameter transparent pipes.

4.1.3 Flow Regime Observations and Map Characteristics

The flow pattern evolution of low-temperature CO_2 two-phase flow exhibits characteristics closely related to its unique thermophysical properties. Due to the large gas-liquid density ratio and low surface tension and viscosity of CO_2, its flow behavior tends to be more homogeneous, which simplifies the flow pattern diagram.

In the two-phase CO_2 flow experiment in a 3-inch horizontal pipe, the main flow patterns observed were stratified flow, stratified-turbulent flow, and dispersed phase flow, with no large-scale slug flow observed. The validation results show that the drift flux model can predict the liquid holdup and pressure drop well under these conditions [56].

Experiments on a vertical tube with an inner diameter of 44 mm and a pressure of 6.5 MPa showed that, under most operating conditions especially upflow, the gas and liquid phases exhibited almost no slippage and high homogeneity; however, in downflow, some liquid phase accumulation and flow pattern differences were observed [50].

These observations are in high agreement with the conclusions of the IFE scaling experiment, further confirming that the unique thermophysical properties of CO_2 inhibit interphase slip and make the two-phase flow closer to a uniform flow. Comparative analysis shows that small-scale and pilot/industrial-scale operations maintain consistency in major flow pattern categories and phase interface characteristics. However, in large-diameter pipes, the shear wave instability and gravity effects of stratified flow are more significant, suggesting that existing flow pattern discrimination criteria need to be modified and adjusted when designing large-scale pipes.

5 Phase Change Mechanisms and Coupled Effects

While macroscopic flow regimes describe the observable state of the system, the underlying evolution of the CH_4-CO_2 flow is governed by the intricate coupling between thermodynamics, heat transfer, and fluid mechanics. In cryogenic pipelines, these processes are rarely independent; they interact in dynamic feedback loops that drive the system away from equilibrium.

5.1 Heat and Mass Transfer during Phase Change

The formation of solid CO_2 is not instantaneous. It is a rate-dependent process controlled by the competition between the generation of latent heat and the diffusion of mass.

5.1.1 Convective Heat Transfer

In pipe flow, the condensation and near-critical convective heat transfer behavior of CO_2 exhibits high complexity and is strongly dependent on thermohydraulic parameters such as mass flux, vapor quality, and temperature. Through experimental studies on pure components and mixtures, the modulation mechanism of the heat transfer coefficient by different flow patterns and thermophysical property changes was revealed.

Supercritical or transcritical CO_2 flows in vertical loops exhibit a distinct trend: increasing the mass flux significantly improves the heat transfer coefficient (HTC). As noted in experiments [57,58], the effects of dramatic changes in thermophysical properties are mainly concentrated in a limited range near the critical point. To capture these variations—specifically the sharp peaks in specific heat (C_p) and density gradients near the pseudocritical temperature—constant-property correlations are insufficient. instead, variable-property correlations such as the Jackson correlation are widely adopted to account for buoyancy and acceleration effects in Eq. (3):

$$N_{ub} = 0.0183\mathrm{Re}_b^{0.82}\mathrm{Pr}_b^{0.5}\left(\frac{\rho_{\varpi}}{\rho_b}\right)^{0.3}\left(\frac{\overline{C}_p}{C_{p,b}}\right)^{n} \tag{3}$$

Experiments on CO_2 flow condensation in horizontal tubes indicate that the HTC increases significantly with increasing mass flux and dryness fraction [59]. To model this shear-dominated regime, the general correlation proposed by Shah is applicable. It relates the two-phase enhancement factor to the Convection number, explicitly modeling the impact of vapor quality and pressure (P_{red}), shown in Eq. (4):

$$h_{TP} = h_L\left[(1-x)^{0.8} + \frac{3.8x^{0.76}(1-x)^{0.04}}{{P_{red}}^{0.38}}\right] \tag{4}$$

This mathematical expression aligns with the experimental findings on CO_2-refrigerant mixtures [60, 61], where higher dryness fraction and mass flux remain the dominant factors for increasing the HTC, despite non-monotonic trends with composition.

While the fluid-side mechanism is dominated by convection, the deposition of solid CO_2 (frost) introduces a critical conductive resistance. The formation (Eq. (5)) of a porous "dry ice" layer on the wall acts as an insulator, degrading the overall heat transfer efficiency [62]:

$$\frac{1}{h_{eff}} = \frac{1}{h_{fluid}} + \frac{\delta_{frost}}{k_{frost}} + R_{wall} \tag{5}$$

As the frost thickness (δ_{frost}) increases, the effective heat transfer coefficient (h_{eff}) drops exponentially, a phenomenon distinct from pure fluid condensation.

5.1.2 Latent Heat Effects and Non-Equilibrium Thermodynamics

In the rapid expansion, condensation, or evaporation of CO_2, the release and absorption of latent heat play a decisive role in the temperature distribution and thermodynamic state evolution. This phenomenon acts not merely as a passive thermal property but as an active "energy source term" (S_h) that fundamentally alters the flow trajectory.

The latent heat of sublimation, representing the energy required for the direct solid-to-vapor transition, was experimentally determined as early as 1926 [63]. Modern studies have further focused on the phase change heat transfer mechanism in applications such as cryogenic jet cooling and Martian polar ice models [64,65]. These studies reveal that the sublimation rate is strictly coupled to the heat flux via the Stefan condition as shown in Eq. (6):

$$q''_{net} = \lambda \frac{\partial T}{\partial n}\bigg|_{\text{interface}} = \dot{m}'' \Delta H_{sub} \tag{6}$$

This interface energy balance explains the experimentally observed variations in the indirect sublimation heat transfer coefficient of dry ice, which typically ranges from 70 to 126 W/m^2 K [66]. Explicitly modeling this latent heat source term is crucial; neglecting it fails to capture the significant impact on phase change kinetics and the thermal longevity of the ice layer.

In supersonic nozzle flows, the effect of latent heat is also significant. Experimental data indicates that non-equilibrium condensation of CO_2 can result in a liquid phase mass fraction as high as approximately 18.6% [67]. The enormous latent heat (ΔH_{lv}) released during this rapid nucleation process triggers a significant temperature jump. Mathematically, this deviation from isentropic expansion can be approximated by Eq. (7):

$$\Delta T_{jump} \approx \frac{\Delta H_{lv}}{C_p} \cdot \Delta g \tag{7}$$

where Δg is the condensed mass fraction. This thermal effect not only limits further cooling below the triple point but also forces the fluid to rapidly return to thermodynamic equilibrium through internal heating, thereby altering the overall flow expansion path [67].

5.1.3 Mass Diffusion and Coupled Heat–Mass Transfer Mechanisms

In cryogenic multi-component flows, mass diffusion and heat transfer are not isolated processes but are strongly coupled, rendering traditional isothermal assumptions inadequate. Specifically, the phase transition of CO_2 within a methane-rich environment is strictly governed by localized mass diffusion rates. Microscopic investigations utilizing molecular dynamics [68] demonstrate that dynamic diffusion

coefficients dictate the rate at which CO_2 monomers migrate toward nucleation centers. This migration and subsequent aggregation release significant latent heat, creating a transient thermal field. Ultimately, a critical nonlinear feedback loop emerges: this evolving temperature field continuously modulates intermolecular interaction forces and transport properties, which in turn dynamically alters the overall mass transfer efficiency, condensation kinetics, and subsequent latent heat release.

The primary coupling mechanism arises from the sensitivity of the binary diffusion coefficient (DAB) to temperature. In low-temperature gas mixtures, this relationship typically follows the kinetic theory of gases or empirical correlations like the Fuller-Schettler-Giddings equation (Eq. (8)) [69], where diffusivity scales with temperature according to a power law:

$$D_{AB}(T) = D_0(\frac{T}{T_0})^{1.75}\frac{P_0}{P} \tag{8}$$

This nonlinear dependency implies that in the boundary layer near a cryogenic wall, the local diffusion coefficient can drop by over 50%. The diffusional freezing effect significantly retards the mass transport of CO_2 to the wall, creating a self-limiting mechanism for frost growth that isothermal models cannot predict.

In systems with steep temperature gradients, mass transport is driven not only by concentration gradients but also by temperature gradients. This phenomenon, known as the Soret Effect or thermal diffusion shown in Eq. (9), generates a mass flux component ($\mathcal{J}_T$) directed towards the cold region:

$$J_{CO_2} = -\rho D_{AB}\nabla\omega_{CO_2} - \rho D_T\nabla T \tag{9}$$

where D_T is the thermal diffusion coefficient. In CH_4-CO_2 mixtures, the heavier CO_2 molecules tend to enrich at the cold wall due to the Soret effect [70]. Neglecting this term in cryogenic modeling can lead to an underestimation of the surface CO_2 concentration and the resultant blockage risk.

The heat and mass transfer are further bridged at the phase interface by bulk flow induced by mass transfer and the energy balance (the Stefan Flow). The rapid de-sublimation of CO_2 creates a bulk velocity (v_{Stefan}) perpendicular to the interface, which enhances convective heat transfer but distorts the concentration profile, Eq. (10) illustrate that the transfer of CO_2 drives the gas phase to generate an overall flow perpendicular to the interface (Stefant flow), which is the key equation for analyzing the thermo-mass coupling at the CO_2 sublimation interface:

$$\dot{m}''_{total} = \frac{\rho D_{AB}}{1-\omega_{CO_2}}\frac{\partial\omega_{CO_2}}{\partial n} \tag{10}$$

Simultaneously, the release of latent heat at the interface acts as a dynamic boundary condition that raises the local temperature, suppressing further nucleation [62]. Recent numerical studies on analogous coupled systems have quantified this effect, showing that accounting for full heat-mass coupling reduces the predicted diffusion front velocity by approximately 30% to 50% compared to decoupled isothermal models [71].

5.1.4 Phase Behaviour and CH_4-CO_2 Equilibria at Low Temperature

The phase equilibrium behavior of the low-temperature CH_4-CO_2 system forms the thermodynamic basis for multiphase flow research. At low temperatures, this system exhibits complex vapor-liquid-solid regions. Pressure increases at fixed low temperature reduce CO_2 content in both phases, more strongly in

the liquid; added N_2 shifts liquid-region temperatures downward and broadens solid-containing regions, important for predicting hydrate/solid formation during low-temperature processing [72].

In addition to the basic thermodynamic phase equilibrium, the flow behavior of low-temperature CO_2 and CH_4-CO_2 systems is also jointly controlled by the aforementioned kinetic mechanisms such as convective heat transfer, latent heat release, non-equilibrium effects, and heat-mass coupling, as shown in Table 3 below.

Table 3: Summary Table: Mechanisms in CO_2/CH_4-CO_2 Low-T Systems.

Mechaisms		Ref.
Convective Heat Transfer	Increases with increasing mass flux and steam quality; decreases with decreasing saturation temperature; significantly affected by annular flow.	[59–61]
Latent-heat release	Causes temperature jumps, limits over-cooling, feeds back on pressure/leakage	[67,73]
Heat–mass coupling	Cooling reduces CO_2 diffusivity and front speed; heat transfer changes total uptake	[71]
Low-T CH_4-CO_2 phase behavior	Rich VLE/SVE/SLE; pressure strongly reshape CO_2 solubility and solid regions	[28,72,74]

5.2 Solid-Liquid-Gas Interactions

Utilizing the sublimation/solidification properties of CO_2 at low temperatures to form a solid phase (dry ice) for CO_2/CH_4 separation is an important emerging technology in the field of natural gas and biogas purification. However, the introduction of solid particles significantly increases the complexity of the system. A thorough understanding of the impact of dry ice particles on the hydraulics, heat transfer processes, and phase equilibrium characteristics of CO_2-CH_4 (and multi-component) systems is a crucial prerequisite for preventing pipeline blockage, optimizing separation equipment performance, and achieving industrial-scale design.

5.2.1 Phase Equilibrium and Solid Phase Formation

Regarding the core issues of phase equilibrium and solid-phase formation, existing research has established various solid-fluid phase equilibrium models describing CO_2 solidification, covering everything from basic CO_2-CH_4 binary systems to complex ternary systems containing impurities such as H_2S. To accurately capture the solid-phase boundary, specialized equations of state (EOS) for solid-phase regression or modification must be employed. For example, the application of PR-HV, PPR78 models, and improved Peng-Robinson correlations has been proven to be essential for accurately predicting multiphase coexistence regions such as solid-vapor equilibrium (SVE), solid-liquid equilibrium (SLE), and solid-liquid-vapor equilibrium (SLVE) [29,72,75,76].

5.2.2 Transport Characteristics of Dry Ice Particles

In cryogenic CO_2-CH_4 separation and refrigeration systems, the formation of dry ice particles is merely the beginning of the phase change process; subsequent particle transport involves complex dynamic behaviors. The trajectory of solid particles in the flow field does not simply follow the airflow, but is accompanied by interactions such as agglomeration, wall deposition, and re-entrainment. Therefore, the existence of dry ice particles in the flow field is not static, but a dynamic process dominated by a "deposition-re-entrainment" cycle:

In an expanding liquid CO_2 jet, initially, tiny particles of about 1 μm are generated. These particles readily deposit on the wall to form a loose layer, which is then sheared off by the fluid and re-entrapped back into the flow field, agglomerating into large particles on the order of 100 μm. Experiments show that

the agglomerate size is directly proportional to the pipe diameter (Fig. 14) and nozzle diameter (Fig. 15), and inversely proportional to the flow velocity, indicating that the flow velocity and channel size jointly control the balance between deposition and re-entrainment [77,78].

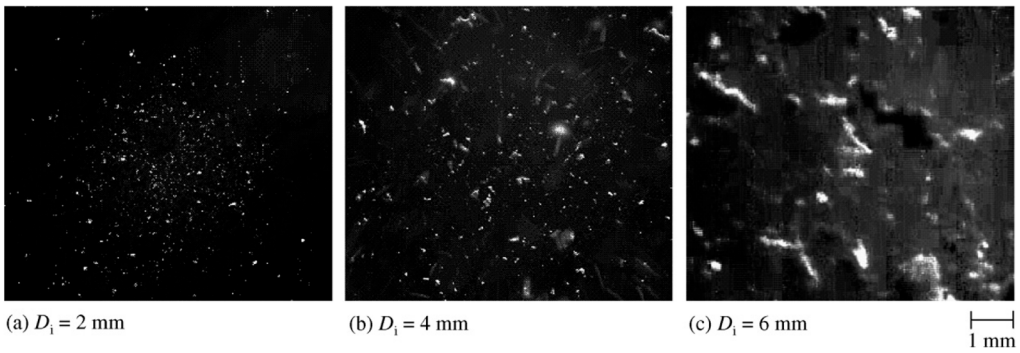

Figure 14: Effect of tube diameter on agglomerate formation. (**a**) Tube diameter = 2 mm; (**b**) Tube diameter = 4 mm; (**c**) Tube diameter = 6 mm. Reprinted with permission from Ref. [77]. Copyright © 2010 The Society of Powder Technology Japan.

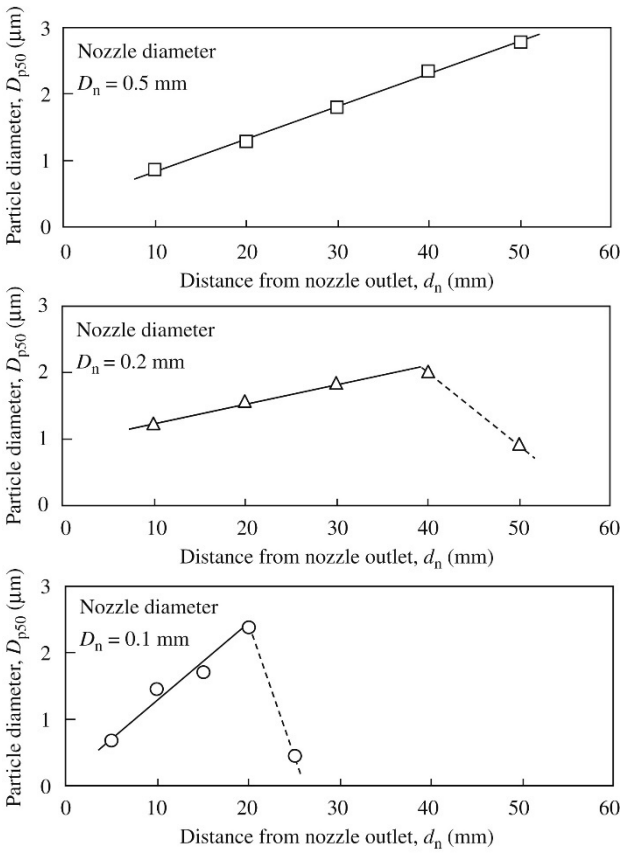

Figure 15: Effect of nozzle diameter on mass median diameter of dry ice particles. Reprinted with permission from Ref. [78]. Copyright © 2012 Elsevier Ltd.

In cooling/refrigeration systems, dry ice tends to deposit and agglomerate at the bottom of the evaporator. Large agglomerates can form dry ice embolisms, causing increased pressure drop and interrupted

intake. Introducing conical channels and cyclones can achieve a more uniform distribution of the solid-gas two phases, significantly mitigating deposition and improving the heat transfer coefficient [79].

5.2.3 Duality of Heat Transfer Characteristics

The effect of solid CO_2 particles on heat transfer exhibits a significant flow-regime dependence, displaying a dual characteristic of both enhancement and deterioration:

In a dispersed flow, fine particles enhance the specific heat capacity and turbulent disturbance of the fluid, contributing to an improved overall heat transfer coefficient [79]. However, once agglomeration or the formation of a moving bed occurs, the heat transfer mechanism undergoes a qualitative change. The accumulated solid layer transforms the dominant heat transfer mode into an inefficient conduction-dominated mode, leading to the formation of localized hot spots and a significant hysteresis in temperature response, the hysteresis time can be up to four times that of uniform flow [80,81].

This nonlinear characteristic suggests that the design of cryogenic heat exchangers should not only focus on macroscopic temperature differences but also on local flow pattern control. The dominant role of solid-phase thermal conductivity (~0.25 W/m·K) in porous media further confirms this: the solid-phase packing structure is the bottleneck determining macroscopic heat transfer efficiency [82].

Current research demonstrates a solid thermodynamic foundation, but fragmented studies on multi-field coupling are lacking: Thermodynamically: Existing literature accurately characterizes the solid-fluid-vapor phase equilibrium envelope of impurity-containing CO_2-CH_4 systems, providing a reliable theoretical basis for predicting dry ice formation and separation windows. Kinetically: While the "deposition-re-entrainment" mechanism in jets and heat exchangers and its dual impact on local heat transfer are clear, very few studies have integrated the coupling of "solid-liquid-gas three-phase flow hydrodynamics + phase change heat transfer + wall adhesion." Existing conclusions are mostly based on liquid-phase water/hydrate systems or pure CO_2 transport; extrapolating them directly to low-temperature CO_2-CH_4 binary slurry systems requires extreme caution.

6 Modeling and Simulation Methods

The prohibitive costs and limited operational scope associated with experimental measurements have rendered the development of high-precision theoretical prediction models imperative. Driven by advancements in experimental techniques and computational capabilities, thermodynamic modeling for cryogenic CH_4-CO_2 systems has evolved through three distinct phases: the modification of classical cubic Equations of State (EOS), the adoption of complex molecular simulations grounded in microscopic mechanisms, and the recent emergence of artificial intelligence and data-driven methodologies.

6.1 Equations of State and Physical Property Calculation Models

Classical cubic equations of state (EOS), like Peng–Robinson (PR) and Soave–Redlich–Kwong (SRK), are widely used for phase equilibrium calculations but require specific modifications to accurately predict solid-fluid equilibria at low temperatures [83,84], key strategies include adjusting binary interaction parameters (BIPs), employing advanced mixing rules, and integrating solid-phase fugacity models or empirical correlations. These modifications address the limitations of classical EOS in representing the complex behavior of CO_2-rich systems, especially in the presence of impurities and under cryogenic conditions. Recent studies also explore hybrid and association models, such as Cubic-Plus-Association (CPA) and SAFT-type EOS, to further enhance predictive capabilities.

Generally, semi-empirical equations of state are established using pure component data by defining mixing rules to evaluate the average parameters required for equation of state calculations [85]. The attractive parameter (amix) typically incorporates a binary interaction parameter (k_{ij}) to correct the geometric mean assumption. For simple non-polar mixtures, k_{ij} is often assumed to be zero or a constant. However, for the CH_4-CO_2 system, the significant difference in quadrupole moments and molecular sizes necessitates a non-zero k_{ij} to accurately capture the phase behavior, especially in the cryogenic region [84]. As illustrated in Fig. 16, Wibawa et al. demonstrated the critical role of this parameter; by optimizing k_{ij}, they successfully reduced the average absolute deviation (AAD) of calculated frost points to as low as 0.26%, yielding a significantly improved agreement with experimental data [86].

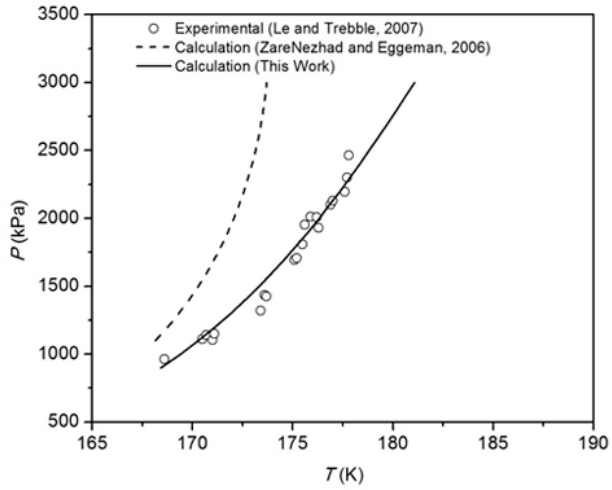

Figure 16: Comparison of calculated frost points using present and literature k_{ij} with experimental data. Reprinted from Ref. [86].

Early studies often treated k_{ij} as a constant tuned to specific isotherms. However, a constant k_{ij} fails to represent the system over a wide temperature range. To address this, recent modeling efforts have adopted temperature-dependent correlations, typically taking a quadratic or linear form (k_{ij} = a + bT + cT_2) By regressing these coefficients against high-precision experimental data, the deviation in bubble/dew point predictions can be reduced to within experimental uncertainty [87]. Studies show that tuning BIPs values for the PR EOS reduced average absolute deviations in solid-vapor equilibrium temperature predictions from over 2% to less than 0.5%. Therefore, the modification of k_{ij} directly impacts the predicted solubility limits and frost point temperatures. As shown in Fig. 17, a poorly tuned k_{ij} can lead to significant errors in predicting the onset of blockage in cryogenic pipelines [85].

Beyond the governing equations, phase discrimination algorithms have undergone continuous evolution. De Guido and Spatolisano [88] developed a multiphase flash algorithm coupled with phase stability analysis to autonomously discriminate between gas-liquid two-phase regions and three-phase zones involving solid CO_2, effectively resolving phase ambiguity issues characteristic of cryogenic conditions. Nikolaidis et al. [89,90] established a generalized Solid-Liquid-Gas Equilibrium (SLGE) computational framework, successfully extending its application to methane-long chain alkane mixtures and CO_2-bearing binary systems. Lasala et al. [91] proposed a hybrid model integrating the PR equation with residual Helmholtz free energy functions. Employing the PR equation for phase equilibrium while leveraging Helmholtz functions to correct thermophysical properties such as density, this model achieves density

prediction errors below 1% for complex CO_2-N_2-CH_4 mixtures and accurately captures abrupt heat capacity variations within the critical region.

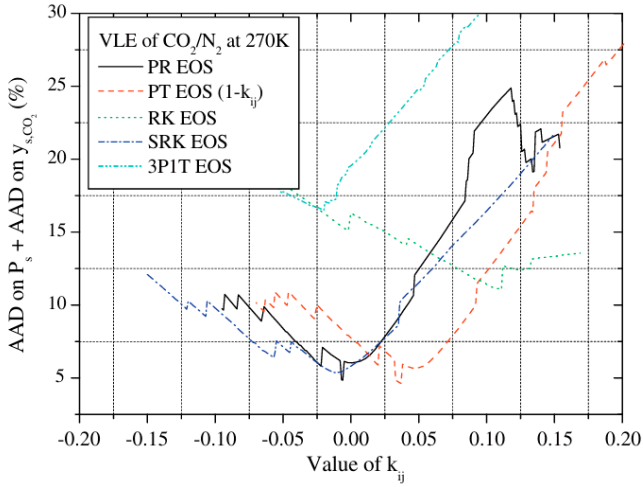

Figure 17: Relationship between calculation accuracy and binary interaction parameter. Reprinted with permission from Ref. [85]. Copyright © 2008 Elsevier Ltd.

The expansion of investigations into extreme operating regimes (high pressure, cryogenic) and complex systems has exposed the inherent limitations of traditional empirical equations. Consequently, methodologies grounded in Statistical Associating Fluid Theory (SAFT) and Molecular Dynamics (MD) have garnered significant attention due to their robust physical underpinnings [26,88,92]. By coupling the SAFT-VR Mie equation with molecular dynamics simulations, Sharifipour and Nakhaee [93] accurately predicted the thermophysical properties of CH_4-CO_2 mixtures across extensive temperature and pressure ranges. Their analysis revealed that the Mie potential function captures the quadrupole effects of CO_2 molecules more effectively than the conventional Lennard-Jones (L-J) potential, thereby enhancing prediction accuracy for vapor-liquid coexistence densities. Zuo et al. [94] applied the $SAFT_2$ equation to the quaternary CH_4-CO_2-H_2O-NaCl system, successfully characterizing CO_2 phase behavior in depleted reservoirs and noting that the salting-out effect on CO_2 solubility diminishes as pressure increases. In a parallel study, Míguez et al. [95] leveraged the SAFT-VR approach to probe the microscopic phase behavior of CO_2-bearing binary mixtures. Addressing high-pressure electrolyte systems, the Electrolyte CPA equation developed by Courtial et al. [96] resolved the inability of conventional models to account for the salting-out effect. Under high-pressure cryogenic conditions, hydrate formation constitutes a critical risk in multiphase flow. Based on statistical mechanics, Algaba et al. [74] employing Monte Carlo (MC) simulations, revealed that neglecting intermolecular dispersive interactions results in a significant underestimation of three-phase equilibrium pressures; incorporating dispersion corrections reduced deviations between predicted and experimental values to within 5%. In porous media, fluid phase behavior is modulated by confinement effects. Xiong et al. [97] proposed a generalized EOS for associating fluids in nanopores, finding that CO_2 phase transition pressures decrease significantly when pore diameters fall below 10 nm. Research by Zhang et al. [98] demonstrates that in shale pores, the competitive adsorption advantage of CO_2 over CH_4 intensifies with increasing pressure, providing a thermodynamic basis for the feasibility of CO_2-enhanced shale gas recovery.

In domains characterized by data scarcity or intractable physical modeling complexities, the implementation of Artificial Intelligence and meta-heuristic optimization algorithms has significantly enhanced predictive accuracy [99,100]. Ali et al. [99] developed an Artificial Neural Network model specifically for predicting gas-liquid-solid equilibria in CH_4-CO_2 binary systems. Trained on extensive experimental datasets, this model achieved a Mean Squared Error of merely 1.2×10^{-4} for three-phase coexistence points, demonstrating superior robustness over traditional EOS, particularly in capturing non-linear behaviors within the near-critical region. Lazzús [100] introduced a hybrid evolutionary algorithm—the Frankenstein PSO—to optimize parameters for binary solid-vapor equilibria, enhancing convergence speeds by approximately 30% compared to conventional gradient descent methods. Applying Response Surface Methodology (RSM), Ahmed [26] performed multi-objective optimization modeling for cryogenic CO_2 removal, defining optimal operating windows that balance energy consumption with separation efficiency.

Classical EOS require targeted modifications to accurately model low-temperature CO_2 solid-phase equilibrium. Adjusting BIPs remains the most effective and widely used strategy. Advanced mixing rules and hybrid models further enhance predictive accuracy, particularly in the presence of impurities or non-ideal interactions. While association models like CPA and SAFT offer improved performance for systems with strong intermolecular interactions, their complexity and parameterization requirements can limit their practical application compared to modified cubic EOS. The choice of modification strategy often depends on the system composition, temperature range, and the availability of experimental data for parameter fitting. Although significant progress in thermodynamic modeling, critical challenges persist in accurately simulating multi-component and multiphase systems under extreme conditions. Future research efforts must prioritize extending frameworks to ternary and quaternary mixtures and integrating complex physical effects [75,101].

6.2 Multiphase Flow Simulation Model Strategy

Low-temperature phase change flow involves physical phenomena across scales, from microscopic nucleation to macroscopic slurry transport. Therefore, the selection of a numerical model essentially involves finding a balance between computational efficiency and interface capture accuracy. Existing literature indicates that no single model can cover all operating conditions; in engineering practice, models are typically selected in a hierarchical manner from three frameworks: Eulerian-Eulerian, Eulerian-Lagrange, and mixed/phase-field, based on the volume fraction of the dispersed phase and the intensity of the phase change.

The E-E framework, which treats each phase as a continuous medium, has always been the preferred solution for simulating industrial-grade pipeline flow, pumping, and slurry flow due to its stability in high-volume-fraction conditions [102,103]. Although traditional E-E methods struggle to capture the local details of discrete particles, the introduction of quasi-multiphase methods has demonstrated excellent engineering applicability in describing the breakup and phase transition of continuous liquid columns during the initial stages of spraying [104].

Eulerian-Lagrange (E-L): A high-fidelity E-L method for tracking nonequilibrium phase transitions, offering significantly higher physical fidelity than E-E in dilute phase flows by tracking discrete particle trajectories [105–107]. The advantage of this method is that it can accurately record the thermal history of individual particles/bubbles, which is crucial for non-equilibrium nucleation and growth processes. However, its accuracy is highly dependent on the two-way coupled closed model and the filtering scale.

Studies have shown that the point particle model still has significant error risks in sub-grid scale modeling, and the high computational cost limits its application in large-scale dense flows [106,108].

For complex interface-driven phase transitions, phase-field methods based on the Cahn-Hilliard or Allen-Cahn equations have demonstrated a powerful ability to capture multi-interface topological changes [109]. To strike a balance between accuracy and cost, academia is increasingly turning to "hybrid Eulerian-Lagrange" or "multi-scale coupling" frameworks, such as using interface tracking in the near field and homogenization models in the far field. These hybrid strategies have proven to be the most promising approach for solving multiphase flow problems across scales [110,111].

To accurately capture CH_4-CO_2 phase transitions under deep-cooling conditions, recent advances have shifted towards multi-scale and data-driven methodologies, significantly overcoming the limitations of traditional models.

In macroscopic Computational Fluid Dynamics (CFD), recent methodologies excel at capturing complex phase transitions under extreme pressure drops. For near- and supercritical two-phase CO2 flows, researchers [112] developed a hybrid mixture model integrating a two-fluid concept with a barotropic approach. This efficiently handles transcritical vaporization and condensation, achieving remarkable precision with pressure and temperature errors restricted to 2–4% and <1%, respectively. Furthermore, to address transient non-equilibrium condensation, advanced CFD frameworks [113] incorporate real-gas equations of state (EOS) alongside modified droplet growth models. This enables the quantitative capture of the precise condensation onset location and nucleation peaks within supersonic nozzles. Together, these high-fidelity advancements provide a robust numerical foundation for optimizing cryogenic natural gas decarbonization.

To resolve the microscopic kinetic triggers that CFD inherently ignores, Molecular Dynamics (MD) is utilized to quantify intermolecular forces. Accurate prediction of cryogenic vapor-liquid-solid (V-L-S) phase equilibria heavily depends on the selected interaction potentials. Recent evaluations demonstrate that the SAFT-VR Mie potential significantly outperforms traditional force fields (e.g., OPLS-UA and UFF) in capturing phase envelopes and thermodynamic properties [93]. Furthermore, accurately modeling the mixture's complex phase behavior often necessitates combining specialized models—such as TraPPE-EH for CH_4 and EPM2 for CO_2—with customized mixing rules or binary interaction parameters [114]. while *ab initio*-derived force fields offer superior predictions for transport properties like self-diffusion [115]. Under specific thermodynamic ensembles (e.g., NVT/NPT), MD studies [42,47] demonstrated that homogeneous CO_2 nucleation is fundamentally governed by the sharp reduction of Lennard-Jones energy and monomer collision rates. Furthermore, by calculating the fluid-solid kinetic interaction energy, MD successfully quantifies how interfacial wettability dramatically lowers the heterogeneous nucleation barrier, providing essential high-precision parameters to correct classical macroscopic flow models.

Finally, Machine Learning (ML) is emerging as a powerful surrogate to bypass computationally expensive thermodynamic iterations. Researchers [99,116] have successfully deployed Artificial Neural Networks (ANN) and hybrid ML models to accurately map the highly non-linear vapor-liquid-solid (V-L-S) phase boundaries of CH4-CO2 mixtures. By training on extensive equilibrium datasets, these data-driven algorithms enable instantaneous prediction of phase stability and flow regime transitions, drastically accelerating the optimization of natural gas decarbonization processes.

To provide practical guidance for numerical model selection, Table 4 summarizes the characteristics, specific applicability to CH_4-CO_2 phase-change flows, and inherent theoretical limitations of these mainstream modeling strategies.

In summary, the numerical simulation strategy for low-temperature CH_4-CO_2 multiphase flow is undergoing a critical paradigm shift from isolated macroscopic modeling to multi-scale coupling and data-driven integration. While conventional CFD frameworks, such as Eulerian-Eulerian (E-E) and Eulerian-Lagrange (E-L) methods, establish the foundation for simulating large-scale transport and capturing basic multiphase hydrodynamics, they inherently struggle with the transient non-equilibrium thermodynamics and microscopic kinetic triggers inherent in deep-cooling phase transitions. Consequently, the most promising and robust simulation strategy involves a synergistic macro-micro-data framework. By employing advanced CFD equipped with real-gas models for precise macroscopic flow tracking, utilizing MD to fundamentally quantify interfacial kinetics and correct classical nucleation barriers, and deploying ML algorithms as highly efficient surrogates for complex phase boundary predictions, researchers can achieve an optimal balance between computational efficiency and physical fidelity. Ultimately, this comprehensive cross-scale simulation strategy not only decodes the underlying mechanisms of solid-liquid-gas interactions but also provides an indispensable theoretical tool for the optimization and risk management of modern natural gas decarbonization technologies.

Table 4: Qualitative comparison of multiphase flow modeling strategies for cryogenic CH_4-CO_2 systems.

Modeling Strategy	Key Characteristics	Applicability	Limitations
E-E	Interpenetrating continuous media with phase-change source terms.	Macro-scale Flow Bulk slurry transport and overall hydrodynamics in large pipelines.	Ignores particle-level thermal history and microscopic nucleation; relies on empirical closures.
E-L	Solves continuous fluid field while tracking discrete particles.	Transient Dynamics Tracking precise trajectory and growth of discrete CO_2 particles during early phase transitions.	High computational cost limits use to dilute suspensions; unsuited for dense flows.
Interface Tracking (VOF/Phase-field)	High-resolution tracking of dynamic interface topological changes.	Local Interface Evolution Capturing intense boundary deformation during supersonic Joule-Thomson expansion.	Computationally prohibitive for bulk particulate flows; heavily restricted by grid resolution.
MD	Microscopic particle tracking driven by intermolecular potentials.	Micro-kinetic Mechanisms Revealing nucleation barriers, collision rates, and fluid-solid interaction energies.	Confined to nano-scale and nano-second domains; incapable of macro-scale flow simulation.
ML	Data-driven models trained on extensive equilibrium datasets.	Instantaneous Prediction Rapidly mapping non-linear V-L-S phase boundaries without thermodynamic iterations.	Accuracy strictly bounded by training data; lacks underlying physical interpretability.

7 Practical Engineering Implications

To translate the aforementioned theoretical mechanisms into industrial flow assurance, clear operational boundaries and early warning indicators are required. (1) Operational Boundaries: Operators should implement dynamic boundaries rather than static thresholds. For LNG heat exchangers, maintaining a CO_2 concentration below 50 ppm and securing a thermodynamic margin above the frost point is crucial. However, this boundary carries uncertainty and must be continually adjusted if trace impurities (e.g., N_2, C_2H_6) are present, as they significantly shift the phase envelope. (2) Early Warning Indicators: Traditional

pressure monitoring is often too delayed for blockage prevention. A sudden localized degradation in the heat transfer coefficient (HTC) serves as a much more sensitive early warning for dry ice deposition. The subsequent onset of non-linear pressure fluctuations confirms the transition from a suspended slurry to a problematic moving bed. These coupled indicators provide a practical basis for real-time risk management in CH_4-CO_2 pipeline networks.

8 Conclusion

This review provides a systematic synthesis of the gas-liquid-solid multiphase flow characteristics of CH_4-CO_2 mixtures in cryogenic pipelines, integrating perspectives from thermodynamic phase equilibrium, microscopic phase change kinetics, and macroscopic hydrodynamics. Key conclusions are summarized as follows:

1. Complexity of Phase Equilibria: Cryogenic CH_4-CO_2 systems exhibit pronounced thermodynamic non-ideality. While classical Equations of State (e.g., Peng-Robinson) remain foundational, accurate prediction of the frost line and solid-phase boundaries strictly requires cryogenically calibrated binary interaction parameters (k_{ij}) or the integration of high-precision Helmholtz free energy models.
2. Predominance of Kinetic Non-Equilibrium Effects: In transient pipeline flows, phase transitions are kinetically constrained by localized subcooling, mass diffusion resistances, and latent heat release. The resulting solid CO_2 particles exhibit dual hydrodynamic effects: uniform dispersion enhances thermal-fluid mixing, while severe agglomeration critically alters the bulk flow regime and slurry viscosity.
3. The Shift in Simulation Paradigms: Resolving these complex coupled effects requires moving beyond isolated macroscopic models. The field is currently experiencing a critical paradigm shift towards multi-scale and data-driven integration, utilizing Molecular Dynamics (MD) to correct classic nucleation barriers and Machine Learning (ML) to accelerate complex phase boundary predictions.

Future Challenges and Outlook:

To further advance the safety and efficiency of cryogenic natural gas decarbonization infrastructure, future research must address several critical challenges:

1. High-Fidelity Visual Experimentation: Developing advanced, high-pressure visual observation techniques to directly quantify bulk slurry hydrodynamics and particle agglomeration kinetics, overcoming current limitations in opaque cryogenic environments.
2. Dynamic Flow Regime Mapping: Constructing transient, multi-phase flow regime maps specifically tailored for the extreme thermal non-equilibrium and rapid expansion conditions typical of CH_4-CO_2 phase changes.
3. Cross-Scale Algorithmic Coupling: Establishing computationally efficient algorithms that seamlessly couple MD-derived microscopic kinetic parameters directly into macroscopic CFD solvers for real-time, industrial-scale flow assurance prediction.
4. Industrial Scale-up and Flow Assurance Integration: Bridging the critical gap between lab-scale kinetic observations and macro-scale pipeline networks. Future frameworks must focus on translating micro-scale non-equilibrium and delayed nucleation models into computationally efficient sub-grid parameters. Integrating these refined kinetic models directly into system-level macroscopic flow assurance strategies will be paramount for optimizing real-time risk management in industrial LNG and CCUS infrastructure.

Acknowledgement: None.

Funding Statement: The authors acknowledge financial support from the National Natural Science Foundation of China (Grant No. 52504062) and the Science and Technology Department of Sichuan Province (Grant No. 2024JDRC0090).

Author Contributions: The authors confirm contribution to the paper as follows: Ting He conceived the review framework and supervised the overall study; Dong Chen conducted the literature search, performed the thematic synthesis and analysis, and drafted the manuscript; Liqiong Chen and Kun Huang contributed to the study conception, provided critical intellectual input, and revised the manuscript; Haoyu Jia assisted with literature screening and prepared the figures and tables. All authors reviewed and approved the final version of the manuscript.

Availability of Data and Materials: The authors confirm that the data supporting the findings of this study are available within the article and properly referenced.

Ethics Approval: Not applicable.

Conflicts of Interest: The authors declare no conflicts of interest.

References

1. International Energy Agency. Net zero by 2050 [Internet]. Paris, France: IEA; 2021 [cited 2026 Jan 1]. Available from: https://www.Iea.Org/reports/net-zero-by-2050.
2. Mohammad N, Mohamad Ishak WW, Mustapa SI, Ayodele BV. Natural gas as a key alternative energy source in sustainable renewable energy transition: A mini review. Front Energy Res. 2021;9:625023. [CrossRef].
3. International Energy Agency. Energy Technology Perspectives 2020—Special Report on Carbon Capture Utilisation and Storage: CCUS in Clean Energy Transitions. Paris, France: OECD publishing; 2020.
4. Bassioni G, Klein H. Liquefaction of natural gas and simulated process optimization—A review. Ain Shams Eng J. 2024;15(2):102431. [CrossRef].
5. Shahzad Kamal M, Sultan AS. Enhanced oil recovery. In: Cellulose-Based Superabsorbent Hydrogels. Cham, Switzerland: Springer International Publishing; 2018. p. 1–33. [CrossRef].
6. Lin K, Wei N, Jiang D, Zhang Y. Progress and perspectives in source-sink matching for CCUS: A critical review. Renew Sustain Energy Rev. 2026;226:116313. [CrossRef].
7. Baena-Moreno FM, Gallego LM, Vega F, Navarrete B. Cryogenic techniques: An innovative approach for biogas upgrading. In: Aryal N, Mørck Ottosen LD, Wegener Kofoed MV, Pant D, editors. Emerging technologies and biological systems for biogas upgrading. Cambridge, MA, USA: Academic Press; 2021. p. 159–86. [CrossRef].
8. Hidalgo D, Martín-Marroquín JM. Cryogenic technologies for biogas upgrading: A critical review of processes, performance, and prospects. Technologies. 2025;13(8):364. [CrossRef].
9. Wanison R, Hadi Syahputra WN, Kammuang-lue N, Sakulchangsatjatai P, Terdtoon P, Tippayawong N, et al. A review of cryogenic carbon capture research: Experimental studies, simulations, and application potential. Therm Sci Eng Prog. 2025;61:103562. [CrossRef].
10. Jing Y, Raffa P, Druetta P. Nano-technologically boosted CO_2-EOR techniques: A review of theoretical, experimental, and field aspects. Chem Eng J. 2025;526:171134. [CrossRef].
11. Davis JA, Rodewald N, Kurata F. Solid-liquid-vapor phase behavior of the methane-carbon dioxide system. AlChE J. 1962;8(4):537–9. [CrossRef].
12. Webster LA, Kidnay AJ. Vapor–liquid equilibria for the methane–propane–carbon dioxide systems at 230 K and 270 K. J Chem Eng Data. 2001;46(3):759–64. [CrossRef].
13. Bi Y, Ju Y. Review on cryogenic technologies for CO_2 removal from natural gas. Front Energy. 2022;16(5):793–811. [CrossRef].
14. Donnelly HG, Katz DL. Phase equilibria in the carbon dioxide–methane system. Ind Eng Chem. 1954;46(3):511–7. [CrossRef].
15. Pikaar MJ. A study of phase equilibria in hydrocarbon-CO_2 systems [dissertation]. London, UK: University of London; 1959.

16. Kurata F, Im KU. Phase equilibrium of carbon dioxide and light paraffins in presence of solid carbon dioxide. J Chem Eng Data. 1971;16(3):295–9. [CrossRef].
17. Zhang L, Burgass R, Chapoy A, Tohidi B, Solbraa E. Measurement and modeling of CO_2 frost points in the CO_2–methane systems. J Chem Eng Data. 2011;56(6):2971–5. [CrossRef].
18. Gao T, Shen T, Lin W, Gu A, Ju Y. Experimental determination of CO_2 solubility in liquid CH_4/N_2 mixtures at cryogenic temperatures. Ind Eng Chem Res. 2012;51(27):9403–8. [CrossRef].
19. Souza LFS, Al Ghafri SZS, Fandiño O, Trusler M. Vapor-liquid equilibria, solid-vapor-liquid equilibria and H_2S partition coefficient in (CO_2 + CH_4) at temperatures between (203.96 and 303.15) K at pressures up to 9 MPa. Fluid Phase Equilib. 2020;522:112762. [CrossRef].
20. Wichterle I, Kobayashi R. Vapor-liquid equilibrium of methane-ethane system at low temperatures and high pressures. J Chem Eng Data. 1972;17(1):9–12. [CrossRef].
21. Raposa SM, Tan SP, Grundy WM, Lindberg GE, Hanley J, Steckloff JK, et al. Non-isoplethic measurement on the solid-liquid-vapor equilibrium of binary mixtures at cryogenic temperatures. J Chem Phys. 2022;157(6):064201. [CrossRef].
22. Waage MH, Vlugt TJH, Kjelstrup S. Phase diagram of methane and carbon dioxide hydrates computed by Monte Carlo simulations. J Phys Chem B. 2017;121(30):7336–50. [CrossRef].
23. Aimoli CG, de Carvalho DP, Pessoa Filho PA, Maginn EJ, Abreu CRA. Thermodynamic properties and fluid phase equilibrium of natural gas containing CO_2 and H_2O at extreme pressures typically found in pre-salt reservoirs. J Nat Gas Sci Eng. 2020;79:103337. [CrossRef].
24. Al Ghafri SZS, Forte E, Maitland GC, Rodriguez-Henríquez JJ, Martin Trusler JP. Experimental and modeling study of the phase behavior of (methane + CO_2 + water) mixtures. J Phys Chem B. 2014;118(49):14461–78. [CrossRef].
25. Eniolorunda OV, Chapoy A, Burgass R. Solid-fluid phase equilibria measurement for mixtures of methane, carbon-dioxide and N-hexadecane. In: Proceedings of the SPE Nigeria Annual International Conference and Exhibition; 2021 Aug 2–4; Lagos, Nigeria. [CrossRef].
26. Ahmed A. Cryogenic process optimization for natural gas purification: Predictive modeling of methane–CO_2 solid–vapor phase equilibrium using response surface methodology. ACS Omega. 2024;9(25):27214–21. [CrossRef].
27. Robustillo MD, de Menezes DÉS, de Alcântara Pessôa Filho P. Phase equilibrium of double-guest clathrates of methane and CO_2, ethane, or propane as measured by high-pressure microcalorimetry. J Mol Liq. 2023;387:122609. [CrossRef].
28. Simoncelli APP, Goméz W, Charin RM, Fleming FP, Ndiaye PM, Tavares FW. Phase behavior of systems with high CO_2 content: Experiments and thermodynamic modeling. Fluid Phase Equilib. 2020;515:112574. [CrossRef].
29. Tang L, Li C, Lim S. Solid–liquid–vapor equilibrium model applied for a CH_4–CO_2 binary mixture. Ind Eng Chem Res. 2019;58(39):18355–66. [CrossRef].
30. Han Y, Liu J, Huang L, He X, Li J. Predicting the phase diagram of solid carbon dioxide at high pressure from first principles. npj Quantum Mater. 2019;4:10. [CrossRef].
31. Li J, Sode O, Voth GA, Hirata S. A solid–solid phase transition in carbon dioxide at high pressures and intermediate temperatures. Nat Commun. 2013;4:2647. [CrossRef].
32. Bian J, Yu B, Cao H, Bai H, Cao X, Guo D. Carbon dioxide condensation: Theory, phenomenon and application. Chem Eng J Adv. 2025;24:100954. [CrossRef].
33. Xu J, He T, Lin W. Experimental and theoretical study of CO_2 solubility in liquid CH_4/H_2 mixtures at cryogenic temperatures. J Chem Eng Data. 2021;66(7):2844–55. [CrossRef].
34. Eggeman T, Chafin S. Beware the pitfalls of CO_2 freezing prediction. Chem Eng Prog. 2005;101:39–44.
35. Lei T, Luo KH, Hernández Pérez FE, Wang G, Wang Z, Restrepo Cano J, et al. Study of CO_2 desublimation during cryogenic carbon capture using the lattice Boltzmann method. J Fluid Mech. 2023;964:A1. [CrossRef].
36. Lei T, Luo KH, Hernández Pérez FE, Wang G, Yang J, Restrepo Cano J, et al. Pore-scale study of CO_2 desublimation and sublimation in a packed bed during cryogenic carbon capture. J Fluid Mech. 2024;990:A6. [CrossRef].
37. Wang Z, Wang B, Wang Y, Bian J, Hua Y, Li Q, et al. Condensation processes of carbon dioxide in high-pressure methane gas: A microscopic study of the dynamic behavior of nucleation, dissolution, and crystallization. Energy. 2025;317:134736. [CrossRef].

38. Kvamme B, Aromada SA, Saeidi N, Hustache-Marmou T, Gjerstad P. Hydrate nucleation, growth, and induction. ACS Omega. 2020;5(6):2603–19. [CrossRef].
39. Kalikmanov VI. Classical nucleation theory. In: Nucleation Theory. Dordrecht, The Netherlands: Springer; 2012. p. 17–41. [CrossRef].
40. Abyaneh MY. Thermodynamics of homogeneous and heterogeneous nucleation in the context of electrocrystallization. J Electrochem Soc. 2018;165(3):D142–6. [CrossRef].
41. Lutsko JF, Durán-Olivencia MA. Classical nucleation theory from a dynamical approach to nucleation. J Chem Phys. 2013;138(24):244908. [CrossRef].
42. Cao H, Cao X, Li H, Zhao X, Cai W, Guo D, et al. Nucleation and condensation characteristics of carbon dioxide in natural gas: A molecular simulation perspective. Fuel. 2023;342:127761. [CrossRef].
43. Liu XY. A new kinetic model for three-dimensional heterogeneous nucleation. J Chem Phys. 1999;111(4):1628–35. [CrossRef].
44. Liu XY. Heterogeneous nucleation or homogeneous nucleation? J Chem Phys. 2000;112(22):9949–55. [CrossRef].
45. Zhang Z, Kusalik PG, Guo GJ, Li Y, Huang L, Wu N. Temperature-controlled gas hydrate nucleation in the heterogeneous environment. J Phys Chem Lett. 2025;16(2):667–74. [CrossRef].
46. Zerón IM, Algaba J, Míguez JM, Grabowska J, Blazquez S, Sanz E, et al. Homogeneous nucleation rate of carbon dioxide hydrate formation under experimental condition from Seeding simulations. J Chem Phys. 2025;162(13):134708. [CrossRef].
47. Cao H, Cao X, Cai W, Zhao X, Guo D, Ding G, et al. Exploring the effect of surface wettability on heterogeneous condensation of carbon Dioxide: A molecular dynamics study. J Mol Liq. 2023;388:122693. [CrossRef].
48. Sampson CC, Metaxas PJ, Barwood MTJ, Sinclair-Adamson R, Falloon PE, Stanwix PL, et al. Experimental solid–liquid equilibria and solid formation kinetics for carbon dioxide in methane for LNG processing. AlChE J. 2023;69(4):e18001. [CrossRef].
49. Farokhpoor R, Liu L, Langsholt M, Hald K, Amundsen J, Lawrence C. Dimensional analysis and scaling in two-phase gas–liquid stratified pipe flow–Methodology evaluation. Int J Multiph Flow. 2020;122:103139. [CrossRef].
50. Hammer M, Deng H, Liu L, Langsholt M, Munkejord ST. Upward and downward two-phase flow of CO_2 in a pipe: Comparison between experimental data and model predictions. Int J Multiph Flow. 2021;138:103590. [CrossRef].
51. Li K, Zhou X, Tu R, Xie Q, Jiang X. The flow and heat transfer characteristics of supercritical CO_2 leakage from a pipeline. Energy. 2014;71:665–72. [CrossRef].
52. Munkejord ST, Deng H, Austegard A, Hammer M, Aasen A, Skarsvåg HL. Depressurization of CO_2-N2 and CO_2-He in a pipe: Experiments and modelling of pressure and temperature dynamics. Int J Greenh Gas Control. 2021;109:103361. [CrossRef].
53. Gu S, Li Y, Teng L, Wang C, Hu Q, Zhang D, et al. An experimental study on the flow characteristics during the leakage of high pressure CO_2 pipelines. Process Saf Environ Prot. 2019;125:92–101. [CrossRef].
54. Theologou K, Mertz R, Starflinger J. Experimental investigation of the heat transfer characteristics of CO_2 at supercritical pressures flowing in heated vertical pipes. Int J Heat Mass Transf. 2025;236:126367. [CrossRef].
55. Li T, Wang S, Li J, Dong K, Wen Z. Experimental study of pore-scale flow mechanism of immiscible CO_2 flooding under *in-situ* temperature-pressure coupling conditions. PLoS One. 2025;20(4):e0321527. [CrossRef].
56. Supak K, Bai F, Hoffman E, Lu Y, Noonan H, Witt K. Two-phase CO_2 flow behavior in horizontal piping. In: Proceedings of the International Pipeline Conference. American Society of Mechanical Engineers; 2024 Sep 23–27; Calgary, AB, Canada. p. V005T09A017. [CrossRef].
57. Song R, Feng Y, Yang D, Zeng G, Mei D, Pioro I, et al. Experiments and heat transfer correlation validations of low-parameter region of sCO_2 flow in a long thin vertical loop. Energies. 2024;17(23):6010. [CrossRef].
58. Yang D, Feng Y, Song R, Pioro I, Chen L. Characterization of CO_2 fluid crossing critical region flow and heat transfer in a vertical loop. Part I: Experimental system and basic trends. Appl Therm Eng. 2025;265:125623. [CrossRef].
59. Li P, Chen JJJ, Norris S. Flow condensation heat transfer of CO_2 in a horizontal tube at low temperatures. Appl Therm Eng. 2018;130:561–70. [CrossRef].
60. Wang P, Li M, Wang Q, Dai B, Ma Y, Tian H. Heat transfer and pressure drop of CO_2/R32 mixture in mini-channel. Int J Heat Mass Transf. 2023;200:123406. [CrossRef].

61. Wang P, Li M, Dai B, Wang Q, Ma Y, Dang C, et al. Experimental and analytical investigation of CO_2/R32 condensation heat transfer in a microchannel. Int J Refrig. 2023;145:338–52. [CrossRef].
62. Debnath B, Mukherjee A, Mullick A, Ghoshdastidar S, Ganguly S, Kargupta K. Desublimation based separation of CO_2 inside a cryogenic packed bed: Performance mapping with the spatiotemporal evolution of CO_2 frost. Chem Eng Res Des. 2019;146:166–81. [CrossRef].
63. Maass O, Barnes WH. Some thermal constants of solid and liquid carbon dioxide. Proc R Soc Lond Ser A Contain Pap A Math Phys Character. 1926;111(757):224–44. [CrossRef].
64. Pilorget C, Forget F, Millour E, Vincendon M, Madeleine JB. Dark spots and cold jets in the polar regions of Mars: New clues from a thermal model of surface CO_2 ice. Icarus. 2011;213(1):131–49. [CrossRef].
65. Zhao Y, Zhao H, He K, Qi X, Zeng X, Liu H. Heat transfer mechanism and influence factors in supercritical CO_2 jet impingement cooling under unconventional physical property changes. Phys Fluids. 2025;37(2):025153. [CrossRef].
66. Outokesh M, Mottafegh A, Nouri-Borujerdi A, Dolati S. An Experimental-Theoretical study on heat transfer aspects of indirect Sublimation, for application in CO_2-based refrigeration systems. Therm Sci Eng Prog. 2023;42:101881. [CrossRef].
67. Wen C, Karvounis N, Walther JH, Yan Y, Feng Y, Yang Y. An efficient approach to separate CO_2 using supersonic flows for carbon capture and storage. Appl Energy. 2019;238:311–9. [CrossRef].
68. Cao H, Cao X, Chen J, Zhao X, Ding G, Guo D, et al. Molecular dynamics simulation of the transport properties and condensation mechanism of carbon dioxide. J Nat Gas Sci Eng. 2022;105:104692. [CrossRef].
69. Fuller EN, Schettler PD, Giddings JC. New method for prediction of binary gas-phase diffusion coefficients. Ind Eng Chem. 1966;58(5):18–27. [CrossRef].
70. Bird RB, Stewart WE, Lightfoot EN. Transport Phenomena. New York, NY, USA: Wiley; 1960.
71. Wu X, Liu W, Chen Y, Niu B, Deng C, Xu Y, et al. Simulation study on the coupled heat and mass transfer of CO_2 in a heavy oil-water liquid system based on an improved lattice Boltzmann (LB) method. Fuel. 2024;361:130684. [CrossRef].
72. Campestrini M, Rabino F, Marques D, Atig D, Stringari P, Franzoni G, et al. Experimental investigation of the effect of nitrogen on the phase equilibrium behavior of the CH_4–CO_2 mixture at low temperature for natural and biogas purification. Fluid Phase Equilib. 2022;553:113292. [CrossRef].
73. Yu H, Zhang G, Yan X. Numerical analysis of phase transition effects on CO_2 leakage along a fault during geologic carbon storage. J CO_2 Util. 2025;101:103193. [CrossRef].
74. Algaba J, Blazquez S, Míguez JM, Conde MM, Blas FJ. Three-phase equilibria of hydrates from computer simulation. III. Effect of dispersive interactions in the methane and carbon dioxide hydrates. J Chem Phys. 2024;160(16):164723. [CrossRef].
75. Ababneh H, Al-Muhtaseb SA. An empirical correlation-based model to predict solid-fluid phase equilibria and phase separation of the ternary system CH_4-CO_2-H_2S. J Nat Gas Sci Eng. 2021;94:104120. [CrossRef].
76. Théveneau P, Fauve R, Coquelet C, Mougin P. Measurement and modelling of solid apparition temperature for the CO_2–H_2S–CH_4 ternary system. Fluid Phase Equilib. 2020;509:112465. [CrossRef].
77. Liu YH, Maruyama H, Matsusaka S. Agglomeration process of dry ice particles produced by expanding liquid carbon dioxide. Adv Powder Technol. 2010;21(6):652–7. [CrossRef].
78. Liu YH, Calvert G, Hare C, Ghadiri M, Matsusaka S. Size measurement of dry ice particles produced from liquid carbon dioxide. J Aerosol Sci. 2012;48:1–9. [CrossRef].
79. Yamasaki H, Yamaguchi H, Kizilkan Ö, Kamimura T, Hattori K, Nekså P. Experimental investigation of the effect of solid-gas two-phase flow in CO_2 cascade refrigeration system. Energy Sources Part A Recovery Util Environ Eff. 2023;45(2):3957–69. [CrossRef].
80. Huang Z, Zhang C, Jiang M, Wang H, Zhou Q. Effects of particle velocity fluctuations on inter-phase heat transfer in gas-solid flows. Chem Eng Sci. 2019;206:375–86. [CrossRef].
81. Guo L, Capecelatro J. The role of clusters on heat transfer in sedimenting gas-solid flows. Int J Heat Mass Transf. 2019;132:1217–30. [CrossRef].
82. Vitali M, Biancini G, Marchetti B, Corvaro F. On the sublimation of dry-ice: Experimental investigation and thermal modelling of low-temperatures on a sandy soil. Energies. 2023;16(2):987. [CrossRef].

83. Tomita S, Akatsu S, Ohmura R. Experiments and thermodynamic simulations for continuous separation of CO_2 from CH_4 +CO_2 gas mixture utilizing hydrate formation. Appl Energy. 2015;146:104–10. [CrossRef].
84. Diamantonis NI, Boulougouris GC, Mansoor E, Tsangaris DM, Economou IG. Evaluation of cubic, SAFT, and PC-SAFT equations of state for the vapor–liquid equilibrium modeling of CO_2 mixtures with other gases. Ind Eng Chem Res. 2013;52(10):3933–42. [CrossRef].
85. Li H, Yan J. Evaluating cubic equations of state for calculation of vapor–liquid equilibrium of CO_2 and CO_2-mixtures for CO_2 capture and storage processes. Appl Energy. 2009;86(6):826–36. [CrossRef].
86. Wibawa G, Nafi MFA, Permatasari A, Mustain A. Application of Peng-Robinson equation of state for calculating solid-vapor and solid-liquid equilibrium of CH_4-CO_2 system. Mod Appl Sci. 2015;9(7):177–82. [CrossRef].
87. ZareNezhad B, Eggeman T. Application of Peng–Rabinson equation of state for CO_2 freezing prediction of hydrocarbon mixtures at cryogenic conditions of gas plants. Cryogenics. 2006;46(12):840–5. [CrossRef].
88. De Guido G, Spatolisano E. Simultaneous multiphase flash and stability analysis calculations including solid CO_2 for CO_2–CH_4, CO_2–CH_4–N_2, and CO_2–CH_4–N_2–O_2 mixtures. J Chem Eng Data. 2021;66(11):4132–47. [CrossRef].
89. Nikolaidis IK, Boulougouris GC, Peristeras LD, Economou IG. Equation-of-state modeling of solid–liquid–gas equilibrium of CO_2 binary mixtures. Ind Eng Chem Res. 2016;55(21):6213–26. [CrossRef].
90. Nikolaidis I, Samoili VS, Voutsas EC, Economou IG. Solid–liquid–gas equilibrium of methane–n-alkane binary mixtures. Ind Eng Chem Res. 2018;57(25):8566–83. [CrossRef].
91. Lasala S, Chiesa P, Privat R, Jaubert JN. Measurement and prediction of multi-property data of CO_2-N2-O_2-CH_4 mixtures with the "Peng-Robinson + residual Helmholtz energy-based" model. Fluid Phase Equilib. 2017;437:166–80. [CrossRef].
92. Zhang J, Clennell MB, Chen Y. New analytical thermodynamic models developed for pure H_2, CH_4, CO_2 and H_2 containing mixtures based on molecular simulations. Int J Hydrogen Energy. 2024;69:687–97. [CrossRef].
93. Sharifipour M, Nakhaee A. Prediction of the CH_4-CO_2 mixture properties using SAFT-VR Mie equation of state and molecular dynamics simulations. Mol Phys. 2024;122(17):e2313036. [CrossRef].
94. Zuo Z, Lu P, Zhu C, Ji X. SAFT2 equation of state for the CH_4–CO_2–H_2O–NaCl quaternary system with applications to CO_2 storage in depleted gas reservoirs. Chem Geol. 2024;667:122328. [CrossRef].
95. Míguez JM, Piñeiro MM, Algaba J, Mendiboure B, Torré JP, Blas FJ. Understanding the phase behavior of tetrahydrofuran + carbon dioxide, + methane, and + water binary mixtures from the SAFT-VR approach. J Phys Chem B. 2015;119(44):14288–302. [CrossRef].
96. Courtial X, Ferrando N, de Hemptinne JC, Mougin P. Electrolyte CPA equation of state for very high temperature and pressure reservoir and basin applications. Geochim Cosmochim Acta. 2014;142:1–14. [CrossRef].
97. Xiong W, Zhang LH, Zhao YL, Wu JF, Huang JH, Yao J. A generalized equation of state for associating fluids in nanopores: Application to CO_2-H_2O, CH_4-H_2O, CO_2-CH_4, and CO_2-CH_4-H_2O systems and implication for extracting dissolved CH_4 by CO_2 injection. Chem Eng Sci. 2021;229:116034. [CrossRef].
98. Zhang J, Zhou J, Xian X, Jiang Y, Tang J, Liao Q, et al. Adsorption behavior and thermodynamic analysis of pure and binary CO_2/CH_4 mixture on shale. Gas Sci Eng. 2025;134:205520. [CrossRef].
99. Ali A, Abdulrahman A, Garg S, Maqsood K, Murshid G. Application of artificial neural networks (ANN) for vapor-liquid-solid equilibrium prediction for CH_4-CO_2 binary mixture. Greenh Gases Sci Technol. 2019;9(1):67–78. [CrossRef].
100. Lazzús JA. Modeling of gas–solid equilibrium of binary systems aided by Frankenstein PSO. Comptes Rendus Chim. 2016;19(5):630–8. [CrossRef].
101. Spatolisano E, Pellegrini LA. Solid–liquid–vapor equilibrium prediction for typical helium-bearing natural gas mixtures. J Chem Eng Data. 2021;66(11):4122–31. [CrossRef].
102. Yang F, Dong Z, Da J, Wang J. A comparative performance evaluation of mainstream multiphase models for aerated flow on stepped spillways. Water. 2024;16(23):3529. [CrossRef].
103. Ali A, Yuan J, Si Q, Iqbal S, Yuan S, Yolandani Y, et al. Comprehensive analysis and identification of energy performance and unsteady two-phase flow patterns based on experiments and comparison between two distinct multiphase flow models. Eng Appl Comput Fluid Mech. 2024;18(1):2356218. [CrossRef].
104. Andreini A, Bianchini C, Puggelli S, Demoulin FX. Development of a turbulent liquid flux model for Eulerian–Eulerian multiphase flow simulations. Int J Multiph Flow. 2016;81:88–103. [CrossRef].

105. Gracka M, Rui L, Miranda JM, Student S, Melka B, Ostrowski Z. Red blood cells tracking and cell-free layer formation in a microchannel with hyperbolic contraction: A CFD model validation. Comput Methods Programs Biomed. 2022;226:107117. [CrossRef].
106. Kim J, Apte SV, Balachandar S. An evaluation of two-way coupled Euler–Lagrange methodology through direct comparison with particle-resolved simulations. Phys Fluids. 2024;36(12):123318. [CrossRef].
107. Cao Q, Nastac L. Mathematical investigation of fluid flow, mass transfer, and slag-steel interfacial behavior in gas-stirred ladles. Metall Mater Trans B. 2018;49(3):1388–404. [CrossRef].
108. Balachandar S, Moore WC, Akiki G, Liu K. Toward particle-resolved accuracy in Euler–Lagrange simulations of multiphase flow using machine learning and pairwise interaction extended point-particle (PIEP) approximation. Theor Comput Fluid Dyn. 2020;34(4):401–28. [CrossRef].
109. Aihara S, Takada N, Takaki T. Highly conservative Allen–Cahn-type multi-phase-field model and evaluation of its accuracy. Theor Comput Fluid Dyn. 2023;37(5):639–59. [CrossRef].
110. Fox RO. Recent advances in well-posed Eulerian models for polydisperse multiphase flows. Int J Multiph Flow. 2024;172:104715. [CrossRef].
111. Kamenik B, Vovk N, Elcioglu EB, Sezgin F, Ozyurt E, Karadeniz ZH, et al. Euler–Euler numerical model for transport phenomena modeling in a natural circulation loop operated by nanofluids. Int J Thermophys. 2025;46(3):40. [CrossRef].
112. Romei A, Persico G. Computational fluid-dynamic modelling of two-phase compressible flows of carbon dioxide in supercritical conditions. Appl Therm Eng. 2021;190:116816. [CrossRef].
113. Zhang G, Li Y, Jin Z, Dykas S, Cai X. A novel carbon dioxide capture technology (CCT) based on non-equilibrium condensation characteristics: Numerical modelling, nozzle design and structure optimization. Energy. 2024;286:129603. [CrossRef].
114. Yang Z, Gong M, Zhou Y, Dong X, Li X, Li H, et al. Vapor-liquid equilibria of CH_4, CO_2 and their binary system CH_4 + CO_2: A comparison between the molecular simulation and equation of state. Sci China Technol Sci. 2015;58(4):650–8. [CrossRef].
115. Higgoda UA, Hellmann R, Koller TM, Fröba AP. Self-diffusion coefficient and viscosity of methane and carbon dioxide via molecular dynamics simulations based on new *ab initio*-derived force fields. Fluid Phase Equilib. 2019;481:15–27. [CrossRef].
116. Ma H, Liu J, Zhang Y, Li J, Kan J, Li N. Prediction of phase equilibrium conditions and thermodynamic stability of CO_2-CH_4 gas hydrate. Appl Sci. 2024;14(6):2320. [CrossRef].